

Synthesis of fluorine-containing phosphodiesterase 10A (PDE10A) inhibitors and the in vivo evaluation of F-18 labeled PDE10A PET tracers in rodent and nonhuman primate

Junfeng Li, Xiang Zhang, Hongjun Jin, Jinda Fan, Hubert Flores, Joel S. Perlmutter, and Zhude Tu
J. Med. Chem., **Just Accepted Manuscript** • DOI: 10.1021/acs.jmedchem.5b01205 • Publication Date (Web): 02 Oct 2015

Downloaded from <http://pubs.acs.org> on October 5, 2015

Just Accepted

“Just Accepted” manuscripts have been peer-reviewed and accepted for publication. They are posted online prior to technical editing, formatting for publication and author proofing. The American Chemical Society provides “Just Accepted” as a free service to the research community to expedite the dissemination of scientific material as soon as possible after acceptance. “Just Accepted” manuscripts appear in full in PDF format accompanied by an HTML abstract. “Just Accepted” manuscripts have been fully peer reviewed, but should not be considered the official version of record. They are accessible to all readers and citable by the Digital Object Identifier (DOI®). “Just Accepted” is an optional service offered to authors. Therefore, the “Just Accepted” Web site may not include all articles that will be published in the journal. After a manuscript is technically edited and formatted, it will be removed from the “Just Accepted” Web site and published as an ASAP article. Note that technical editing may introduce minor changes to the manuscript text and/or graphics which could affect content, and all legal disclaimers and ethical guidelines that apply to the journal pertain. ACS cannot be held responsible for errors or consequences arising from the use of information contained in these “Just Accepted” manuscripts.

1 Synthesis of fluorine-containing phosphodiesterase 10A (PDE10A) inhibitors and
2
3 the in vivo evaluation of F-18 labeled PDE10A PET tracers in rodent and
4
5
6
7 nonhuman primate
8

9 Junfeng Li,^a Xiang Zhang,^a Hongjun Jin,^a Jinda Fan,^a Hubert Flores,^b Joel S. Perlmutter^{a,b} and Zhude Tu^{a*}
10
11

12
13
14 ^aDepartment of Radiology, Washington University School of Medicine, St. Louis, MO, 63110, USA.
15

16
17 ^bDepartment of Neurology, Washington University School of Medicine, St. Louis, MO, 63110, USA.
18

19 *Corresponding author
20
21
22
23

24 **Keywords:** Phosphodiesterase 10A (PDE10A) inhibitor, central nervous system (CNS), schizophrenia,
25
26 Huntington's disease, MP-10, positron emission tomography (PET), Fluorine-18.
27
28
29
30
31
32
33
34
35
36
37
38
39
40
41
42
43
44
45
46
47
48
49
50
51
52
53
54
55
56
57
58
59
60

ABSTRACT

1
2
3 A series of fluorine-containing PDE10A inhibitors were designed and synthesized to improve the metabolic
4 stability of [¹¹C]MP-10. 20 of the 22 new analogues had high potency and selectivity for PDE10A: **18a-j**, **19d-j**,
5 **20a-b**, and **21b** had IC₅₀ values <5 nM for PDE10A. Seven F-18 labeled compounds [¹⁸F]**18a-e**, [¹⁸F]**18g**, and
6 [¹⁸F]**20a** were radiosynthesized by ¹⁸F-introduction onto the quinoline rather than the pyrazole moiety of the
7 MP-10 pharmacophore and performed in vivo evaluation. Biodistribution studies in rats showed ~2-fold higher
8 activity in the PDE10A-enriched striatum than non-target brain regions; this ratio increased from 5 to 30 min
9 post-injection, particularly for [¹⁸F]**18a-d** and [¹⁸F]**20a**. MicroPET studies of [¹⁸F]**18d** and [¹⁸F]**20a** in
10 nonhuman primates provided clear visualization of striatum with suitable equilibrium kinetics and favorable
11 metabolic stability. These results suggest this strategy may identify a ¹⁸F-labeled PET tracer for quantifying the
12 levels of PDE10A in patients with CNS disorders including Huntington's disease and schizophrenia.
13
14
15
16
17
18
19
20
21
22
23
24
25
26
27
28
29
30
31
32
33
34
35
36
37
38
39
40
41
42
43
44
45
46
47
48
49
50
51
52
53
54
55
56
57
58
59
60

INTRODUCTION

Phosphodiesterase 10A (PDE10A) is a dual-specificity phosphodiesterase enzyme that is able to hydrolyze both cyclic adenosine monophosphate (cAMP) and cyclic guanosine monophosphate (cGMP) to AMP and GMP, respectively.¹⁻³ PDE10A mRNA is highly expressed in the brain; expression in peripheral tissues, with the exception of the testis, is low.⁴ Both PDE10A mRNA and protein are specifically enriched in the medium spiny neurons (MSNs) of the striatum.⁵ Abnormal striatal levels of PDE10A play a major role in schizophrenia, Huntington's disease, addiction and other neuropsychiatric disorders.⁶⁻⁸

Positron emission tomography (PET) is a preclinical molecular imaging technique which permits quantitative noninvasive measurement of drug disposition and localization in animal models of human disease and an important tool for clinical studies. PDE10A inhibitors have shown promise as therapeutics in preclinical models of human disease, several have progressed to clinical trials.^{7, 9-16} The highly potent ($IC_{50} = 0.37$ nM) and highly selective (>100-fold) PDE10A inhibitor 2-[4-(1-methyl-4-pyridin-4-yl-1*H*-pyrazol-3-yl)-phoxymethyl]-quinoline (MP-10)¹⁷ has been extensively evaluated as a therapeutic inhibitor of PDE10A and has completed several clinical trials in human subjects.¹⁸ [¹¹C]MP-10 (Figure 1) was independently investigated by several groups as a PET tracer for quantifying PDE10A in vivo. Although variable success and significant species differences have been reported in preclinical studies,¹⁹⁻²¹ [¹¹C]MP-10 remains a potentially viable PET tracer for clinical studies. Numerous other ¹¹C- and ¹⁸F-labeled PDE10A inhibitors have been evaluated in preclinical rodent models and although several candidate tracers have proceeded to studies in nonhuman primates and human subjects, the search for a PET tracer with ideal pharmacological properties is ongoing.²²⁻³¹

Although [¹¹C]MP-10 provides a clear anatomic image of the brain with high accumulation in the striatum of nonhuman primates (NHP), tissue time-activity curves in macaques revealed an increasing trend of radioactivity accumulation in both the target region (striatum) and the reference region (cerebellum) which may limit its utility.¹⁹ Our metabolite analysis of [¹¹C]MP-10 suggested that a brain penetrant radiometabolite was formed by *O*-dealkylation of the pyrazole moiety of [¹¹C]MP-10.¹⁹ An additional consideration in the search for an improved PET tracer is that the longer half-life of ¹⁸F places fewer time constraints on production and permits longer scan sessions that usually result in improved target: non-target ratios and higher quality images.

1 Although a potent and selective quinoline analogue of MP-10 was formed by introducing a [^{18}F]fluoroethyl
2 group on the *N*-atom of the pyrazole moiety ([^{18}F]JNJ41510417, Figure 1),^{32,33} slow equilibrium kinetics were
3 reported in rodents and NHPs, possibly due to brain-penetrant radioactive metabolites that accumulate non-
4 specifically in the brain. To overcome this potential liability, we recently ^{11}C -labeled the quinoline moiety
5 instead of the pyrazole moiety of several new PDE10A inhibitors ([^{11}C]1-4, Figure 1).³⁴ We hypothesized that
6 this strategy might lead to the identification of a new analogue with (i) increased *in vivo* metabolic stability,
7 and/or; (ii) a metabolic pathway which generates radioactive metabolites that do not cross the blood-brain
8 barrier (BBB). Our earlier structure-activity relationship (SAR) study explored introduction of a methoxy group
9 (-OCH₃) in the 3, 4 or 6-position of the 2-methylquinoline moiety of the MP-10 pharmacophore and the
10 regioisomers of the new analogues. The most potent and selective compounds were the 3- and 4-methoxy
11 substituted quinolines with an O-atom bridge linkage; little difference was seen in the *in vitro* biological activity
12 of regioisomers.³⁵ Subsequent evaluation of the ^{11}C -labeled lead tracers showed prolonged favorable target:
13 background ratios in rats for the 3- and 4-methoxy substituted quinolines with high selectivity in the target
14 region and non-target region and promising kinetic behavior in both the target region (striatum) and the
15 reference regions of NHPs.³⁴

16 We have continued our exploration of ^{18}F -labeled PET radiotracers for PDE10A by introducing fluoro-,
17 fluoromethyl, fluoropropyl or triazole fluoroethyl groups into the quinoline moiety of MP-10. We also explored
18 the introduction of a short fluoroPEGylated (FPEG) unit. Incorporation of a short FPEG unit has been shown to:
19 (i) enable facile ^{18}F -labeling of the target compound; (ii) improve the *in vivo* pharmacokinetics of molecules
20 interacting with biologically interesting proteins or peptides;^{36,37} (iii) decrease the lipophilicity of molecules,
21 which enhances their ability to cross the BBB.³⁸ Radiolabeling of [^{11}C]MP-10 also yielded the regioisomer
22 ([^{11}C]isoMP-10 Figure 1),¹⁹ a slightly less potent PDE10A inhibitor reported in the discovery of MP-10;¹⁷
23 [^{11}C]isoMP-10 also showed selective binding in the rat striatum, though initial brain uptake was significantly
24 lower than that of [^{11}C]MP-10.²⁸ We further expanded our synthetic efforts to include modification of the
25 pyrazole moiety to generate regioisomers of the new fluorine-containing MP-10 quinoline analogues; this
26 permitted expanded SAR studies. Here we report (i) the synthesis and screening of new analogues which allow

¹⁸F-labeling in the quinoline moiety rather than the pyrazole moiety; (ii) ¹⁸F-labeling of the potent and selective candidates and the in vivo evaluation of their suitability as PDE10A PET imaging agents using rats and macaques.

RESULTS AND DISCUSSION

Chemistry. The syntheses of target new PDE10A analogues was accomplished by a Mitsunobu reaction³⁹ of benzyl alcohols on quinoline moiety coupling with substituted phenols on pyrazole moiety **17a-b**, or a *O*-alkylation of substituted methyl bromide on quinoline moiety with substituted phenols **17a-b**.

Following the above strategy, quinoline fragments of molecules including fluorine-containing intermediates **6a-j** and **15a** were first synthesized as shown in Scheme 1. Different approaches were used for the synthesis of compounds **6a-j** and **15a**: (i) aniline **5** was converted to the aryl fluoride **6a** via diazonium fluoroborates under the Balz-Schiemann conditions⁴⁰; (ii) the alcohol **7** was converted directly into **6b** by treatment with diethylaminosulfur trifluoride (DAST); (iii) treatment of compound **8** with 1,1,1-trifluoro-*N*-phenyl-*N*-((trifluoromethyl)sulfonyl)methane-sulfonamide afforded the triflate. Stille reaction⁴¹⁻⁴³ of the triflate with allyltributyltin in the presence of tetrakis triphenylphosphine palladium and lithium bromide generated compound **9**. Hydroboration-oxidation of **9** to afford the alcohol, followed by fluorination generated compound **6c**; (iv) alkylation of commercially available **10** (ethyl 4-hydroxy quinoline-2-carboxylate) with 2-fluoroethyl bromide afforded ethyl 4-(2-fluoroethoxy)quinoline-2-carboxylate (**6d**) in 60% yield; (v) alkylation of the phenol group of **10** with either a -Cl atom or -OTs group afforded the corresponding alcohols which were converted using DAST to the corresponding fluoroPEGylated intermediates **6e-g** in modest yields (60-71%); (vi) alkylation of (2-methylquinolin-4-yl)methanol **7** with 2-fluoroethyl bromide under basic conditions afforded 4-((2-fluoroethoxy)methyl)-2-methylquinoline **6h**; (vii) the aniline group of **5** was protected using di-*tert*-butyl dicarbonate to form the Boc-protected compound **11**, subsequent *N*-alkylation using 2-fluoroethyl bromide afforded **6i**; (viii): **10** was brominated using POBr₃ to afford ethyl 4-bromoquinoline-2-carboxylate **12**, which was converted to the azide compound and subjected to click reaction conditions,⁴⁴ followed by DAST fluorination to afford compound **6j**; (ix) using Friedlander synthesis⁴⁵, 2-aminobenzaldehyde **13** reacted with 1-

1 methoxypropan-2-one afforded the 3-methoxy-2-methylquinoline⁴⁶, subsequent demethylation utilizing BBr₃
2 followed by *O*-alkylation afforded compound **15a**.
3

4
5 The synthesis of intermediate compounds **16a-n** was accomplished using strategies shown in Scheme 2. (i)
6 bromination of **6a** or **15d** using NBS afforded compound **16a** and **16n** respectively (Scheme 2, Method 1); (ii)
7 the methylquinoline derivatives **6b-c**, **6h-i**, **15a-c** were oxidized using selenium dioxide (SeO₂), followed by
8 NaBH₄ reduction, while the ethyl quinoline-2-carboxylate **6d-g**, **6j** were reduced using NaBH₄ to afford the
9 corresponding alcohols **16b-m** (Scheme 2, Methods 2-3). The detailed methods for synthesis of intermediates
10 are provided in the Supporting Information.
11
12
13
14
15
16
17
18

19 The synthesis of final compounds **18a-j**, **19d-j**, **20a-d**, and **21b** was accomplished as shown in Scheme 3.
20 Substituted phenols **17a-b** were prepared as previously published (Scheme 3).³⁵ **16b-m** were coupled with the
21 phenol **17a** or **17b** with a Mitsunobu reaction³⁹ to afford **18b-j**, **20a-c**, **19d-j** and **21b**. Compounds **18a**, **20d**
22 were made by *O*-alkylation of the substituted phenol **17a** with substituted methyl bromide **16a** or **16n**.
23
24
25
26
27

28 In vitro inhibition assays identified candidate potent and selective analogues for radiolabeling: **18a-e**, **18g**
29 and **20a**. Schemes 4 and 5 outline the synthesis of the precursors for radiolabeling; the detailed methods for
30 their synthesis are provided in the Supporting Information. Scheme 4 outlines the synthesis of precursors **23a**,
31 **23d** and **24a**. The method described above for synthesis of **16d** from **6d** was used for the synthesis of **23a**. A
32 methoxymethyl ether (MOM) group was used to protect phenols **10** and **24b** under basic conditions, the
33 protected intermediates were reacted with the substituted phenol **17a** under Mitsunobu reaction conditions to
34 afford **27a-b**. The MOM ether functional group was easily deprotected by TFA to afford precursors **23d** and
35 **24a**.
36
37
38
39
40
41
42
43
44
45
46

47 The precursors **23b-c**, **23e**, **23g** were obtained by following Scheme 5. Commercially available *tert*-
48 butyldimethylsilyl (TBS) chloride was used as a silylation agent to protect alcohols **28a-d**. The use of 1.7 eq.
49 imidazole as base with 1.7 eq. of TBSCl and DMF as solvent proved effective and resulted in TBS-ethers **29a-d**
50 in high yield. Compounds **29a-d** were converted to the respective alcohols **30a-d**, which were coupled with the
51 phenol **17a** or **17b** in the presence of Ph₃P and di-*tert*-butyl azodicarboxylate (DBAD) via a Mitsunobu *O*-
52 alkylation³⁹ to afford compounds **31a-d**. The TBS-ethers **31a-d** were easily deprotected with a catalytic amount
53
54
55
56
57
58
59
60

of tetrabutyl ammonium fluoride (TBAF), the intermediate alcohol was then chlorinated or sulfonated as indicated in Scheme 5 to afford precursors **23b-c**, **23e**, and **23g**.

Radiochemistry. An overview of the radiolabeling strategies for [^{18}F]**18a-e**, [^{18}F]**18g**, and [^{18}F]**20a** is shown in Scheme 6. These tracers were labeled by the following strategies: (i) a one-step direct nucleophilic halogen exchange was used for labeling [^{18}F]**18a** and [^{18}F]**18b**; (ii) a one-step direct nucleophilic aliphatic substitution with a tosylate (Ts) or mesylate (Ms) leaving group was used for labeling [^{18}F]**18c**, [^{18}F]**18e**, and [^{18}F]**18g**; (iii) a two-step strategy was used for labeling [^{18}F]**18d** and [^{18}F]**20a** using the 2- ^{18}F fluoroethyl tosylate **34** as a secondary labeling agent. The structures of the new fluorine-containing PDE10A inhibitors [^{18}F]**18a-e**, [^{18}F]**18g**, and [^{18}F]**20a** are shown in Figure 2.

Scheme 6 shows the conditions used for the successful radiolabeling of [^{18}F]**18a-e**, [^{18}F]**18g**, and [^{18}F]**20a**. Labeling of [^{18}F]**18b** was initially planned by a direct nucleophilic aliphatic substitution using a tosylate (Ts) or mesylate (Ms) leaving group. However, because heating the precursor with $^{18}\text{F}^-$ at 85 °C for 15 min yielded only a trace of [^{18}F]**18b**, an alternative strategy of halogen exchange reaction was pursued, this was successfully performed using the chloride precursor **23b**. As shown in Scheme 6, a one-step displacement reaction using mesylate and tosylate leaving groups was employed for radiolabeling [^{18}F]**18b**, [^{18}F]**18c**, [^{18}F]**18e**, and [^{18}F]**18g**. A two-step strategy was used for the radiosynthesis of [^{18}F]**18d** and [^{18}F]**20a** using the tosylate [^{18}F]**34** as a secondary labeling agent. First, [^{18}F]KF/4,7,13,16,21,24-Hexaoxa-1,10-diazabicyclo[8.8.8]hexacosane (Kryptofix[222]) was substituted into the di-tosylate **33**. Second, the resulting 2- ^{18}F fluoroethyl tosylate, [^{18}F]**34**, was directly used in a nucleophilic substitution by reaction with the precursors to afford [^{18}F]**18d** and [^{18}F]**20a**. Details are provided in the Experimental section. All tracers were obtained with high specific activity (SA), and with a radiochemical yield sufficient for in vivo studies. The radiochemical purity of each tracer was > 99% and the chemical purity was >95%. Details of the radiosynthesis for each ^{18}F -labeled compound are provided in the Experimental section.

In Vitro Assays. We previously reported that the introduction of a 3- or 4- methoxy group on the quinoline fragment of MP-10 and isoMP-10 yielded potent and PDE10A selective analogues.³⁵ Here we report our continued exploration of fluorine-containing quinoline analogues as PDE10A inhibitors. In vitro potency and

1 selectivity of the new substituted quinoline analogues as PDE10A inhibitors are shown in Table 1; the top
2 section of the table contains analogs of MP-10 while the lower section contains select corresponding
3 regioisomers which are analogues of isoMP-10. Comparison of the in vitro assay results for MP-10 analogues
4
5 **18d-j** and **20b**, with the regioisomers **19d-j** and **21b** showed no significant difference for paired regioisomers,
6
7 although the slightly lower IC_{50} values for the analogues based on MP-10 suggest they may be modestly more
8
9 potent. New analogues with a fluorine-containing group into 4-position of the quinoline moiety of the MP-10
10
11 pharmacophore (**18a-j**, **19d-j**), had high potency for PDE10A with IC_{50} values <3 nM, particularly **18a-b**, **18d-i**
12
13 and **19f-i** with IC_{50} values <1 nM. These results are consistent with the SAR we reported for the methoxy-
14
15 substituted quinolone analogues.³⁵
16
17

18
19
20
21 We also explored substitution at the 3- and 6- positions. Compound **20a** (3-fluoroethoxy substitution)
22
23 demonstrated high PDE10A inhibition ($IC_{50} = 0.26$ nM). Replacement of the hydrogen atom at 6-position of the
24
25 quinoline moiety with fluoride(-F) yielded regioisomers **20b** and **21b** which demonstrated high potency with
26
27 IC_{50} values of 0.29 and 0.76 nM respectively, however, replacement of the hydrogen at 6-position using larger
28
29 fluorine-containing groups resulted in analogues with low potency (**20c**, $-CH_2F$, $IC_{50} > 76$ nM; **20d**, $-$
30
31 OCH_2CH_2F , $IC_{50} = 33.5 \pm 0.08$ nM).
32
33
34

35
36 Selectivity of a PET ligand for PDE10A over the other subtypes is also an important consideration.
37
38 Inhibition of PDE3A/B has been associated with arrhythmia and increased mortality,^{47, 48} while PDE4 is widely
39
40 expressed in the central nervous system.^{49, 50} The potent new PDE10A inhibitors (20 compounds, PDE10A IC_{50}
41
42 <5 nM) were also evaluated for inhibition of PDE3A/B and PDE4A/B. The results for final compounds **18a-j**,
43
44 **19d-j**, **20a-d**, and **21b** (Table 1) revealed almost all compounds had very low potency for inhibiting PDE3A/B
45
46 and PDE4A/B with the IC_{50} value > 750 nM, except **18c** which had slight potency for PDE4A/B (IC_{50} 460 nM
47
48 for PDE4A and 380 nM for PDE4B). All of the new compounds, including **18c**, had >210 -fold selectivity ratios
49
50 for PDE10A vs PDE3A/B and PDE4A/B. This suggests that **18a-j**, **19d-j**, **20a-b** and **21b** are both potent and
51
52 selective inhibitors of PDE10A.
53
54
55

56
57 Based on these screening results and our previous experience with the ^{11}C -labeled regioisomers, seven
58
59 analogues of MP-10 were identified as candidate ligands for ^{18}F -labeling: $-F$ (**18a**), $-(CH_2)_nF$ (**18b**, **18c**), $-$
60

OCH₂CH₂F (**18d**), -CH₂OCH₂CH₂F (**18e**), and -FPEG (**18g**, **20a**). The precursors were synthesized (details are provided in the Supporting Information) for the subsequent radiolabeling and the in vivo evaluation as PET tracers for quantification of PDE10A in rodents and nonhuman primates.

Biodistribution. The biodistribution of [¹⁸F]**18a-e**, [¹⁸F]**18g**, and [¹⁸F]**20a** was evaluated in normal adult male Sprague-Dawley rats at 5, 30 and 60 min post-injection (p.i.) **Table 2** shows the uptake and washout in peripheral organs and whole brain for each of the seven tracers. The initial brain uptake values were 0.410 ± 0.063, 0.128 ± 0.012, 0.114 ± 0.015, 0.118 ± 0.012, 0.213 ± 0.039, 0.353 ± 0.052, and 0.092 ± 0.011 %ID/g for [¹⁸F]**18a**, [¹⁸F]**18b**, [¹⁸F]**18c**, [¹⁸F]**18d**, [¹⁸F]**18e**, [¹⁸F]**18g**, and [¹⁸F]**20a**, respectively. At 5 min, 30 min, and 60 min p.i., brain uptake of each of the tracers was comparable to or higher than [¹¹C]MP-10 (0.162 ± 0.025, 0.066 ± 0.008, and 0.056 ± 0.006 %ID/g 5 min, 30 min and 60 min p.i.).¹⁹ Modest but progressive accumulation of radioactivity in bone was observed for [¹⁸F]**18a**, [¹⁸F]**18b**, and [¹⁸F]**18c**: bone activity increased from 0.522 ± 0.116, 0.421 ± 0.063, and 0.222 ± 0.014 %ID/g at 5 min to 6.300 ± 0.314, 5.620 ± 1.132, and 2.037 ± 0.303 %ID/g at 60 min p.i. respectively. This progressive increase in bone activity was most likely the result of metabolic defluorination. These results suggest that functional groups including -F (**18a**), -CH₂F (**18b**), and -CH₂CH₂CH₂F (**18c**) on the quinoline fragment of MP-10 undergo in vivo metabolic defluorination in rodents. In contrast, [¹⁸F]**18d**, [¹⁸F]**18e**, [¹⁸F]**18g** and [¹⁸F]**20a** appeared more stable to in vivo defluorination.

The cerebellum and cortex are accepted reference (non-target) regions in kinetic modeling of PDE10A PET tracers.²⁹ Therefore, in addition to high striatal uptake and retention, a candidate tracer for clinical imaging should show low uptake and rapid washout in the cerebellum and cortex; this will facilitate high target: non-target ratios and yield high quality images. The new radiotracers displayed generally heterogeneous regional brain distribution with the highest uptake observed in the striatum; by 30 min p.i., the ratio of activity in the striatum versus non-target brain regions was > 2-fold for [¹⁸F]**18a**, [¹⁸F]**18b**, [¹⁸F]**18c**, [¹⁸F]**18d**, and [¹⁸F]**20a** (**Figure 3**). Between 5 and 30 min p.i., the striatum: cerebellum and striatum: cortex ratios increased for the five tracers, which suggests that they were rapidly cleared from non-target regions and displayed specific binding within the PDE10A-enriched-striatum.

Taken together, the rodent biodistribution and regional brain uptake and washout data identified 4-

1 fluoroethoxy [^{18}F]**18d** and 3-fluoroethoxy [^{18}F]**20a** as the more promising candidates for further evaluation in
2 nonhuman primates. Both tracers appeared stable to metabolic defluorination and showed favourable ratios in
3 the striatum versus non-target brain regions.
4
5

6
7 **MicroPET Imaging Studies of Cynomolgus Macaques.** The two fluoroethoxy lead PET radioligands for
8 imaging PDE10A, [^{18}F]**18d** and [^{18}F]**20a**, underwent PET imaging studies ($n = 3$ for each tracer) in male
9 cynomolgus monkeys (**Figure 4**) using a microPET Focus 220 scanner. The representative summed images
10 from 0 to 180 min were co-registered with MRI images to accurately identify the anatomical regions of interest
11 (ROI's) are shown in **Figure 4**. MicroPET studies of both [^{18}F]**18d** and [^{18}F]**20a** gave clear visualization of the
12 PDE10A-enriched striatum. Both the caudate and putamen striatal regions had high uptake of [^{18}F]**18d** and
13 [^{18}F]**20a** ; the ratios of uptake in the striatum vs. non-target brain regions were > 3 -fold by 40 min p.i. In
14 particular, for [^{18}F]**20a**, target: non-target ratios reached > 5 -fold by 70 min p.i. More importantly, although the
15 two tracers showed differences in striatal clearance, tissue time-activity curves of both [^{18}F]**18d** and [^{18}F]**20a**
16 demonstrated improved washout kinetics from both target and non-target regions compared with [^{11}C]MP-10.
17 The improved washout kinetics suggest that the strategy of ^{18}F -labeling the quinoline rather than the pyrazole
18 moiety reduced the formation of radioactive metabolites that cross the BBB.
19
20
21
22
23
24
25
26
27
28
29
30
31
32
33
34
35

36 **Metabolite Studies in Cynomolgus Macaques.** Initial NHP brain imaging of [^{18}F]**18d** and [^{18}F]**20a** showed
37 improved kinetics over previously published PET tracers for PDE10A. To further investigate the in vivo
38 metabolic stability of these tracers, HPLC analysis was performed to identify the percentage of parent
39 compound versus radiometabolites in solvent extracts of NHP plasma obtained during microPET imaging
40 studies of [^{18}F]**18d** and [^{18}F]**20a**. NHP arterial blood was obtained from cynomolgus macaques 5, 15, 30, 60 and
41 90 min p.i for [^{18}F]**18d** and [^{18}F]**20a**. Plasma was separated from packed red cells; ~ 65 -75% of the radioactivity
42 was in the plasma. Following solvent extraction and deproteination, $\sim 90\%$ of the plasma activity was in the
43 supernatant and only 10% of the activity was in the protein pellet. The solvent extract was injected onto an
44 HPLC to quantify the percentage of the radioactivity for the parent compound versus radiolabeled metabolites
45 based on the different retention times. As shown in **Table 3**, HPLC analysis of NHP plasma revealed good
46 metabolic stability for both [^{18}F]**18d** and [^{18}F]**20a**. Particularly, at 30 min p.i., solvent extracts of arterial blood
47
48
49
50
51
52
53
54
55
56
57
58
59
60

1 contained ~90% parent compound for [^{18}F]**18d**. The major radioactive metabolite of [^{18}F]**18d** was more polar
2 (retention time ~3.5 min) than the parent compound (retention time ~10.5 min), negligible amounts of a
3 minor radioactive metabolite (retention time ~7.5 min) were also observed. For [^{18}F]**20a**, solvent extracts of
4 arterial blood contained > 90% parent compound 15 min p.i., 73% parent remained 30 min p.i. The major
5 radioactive metabolite was more polar (retention time ~3.5 min) than the parent compound (retention time ~
6 10.5 min). The minor radioactive metabolite was < 14% of the recovered activity 90 min p.i. (retention time
7 ~7.5 min). The results of the metabolite analysis confirmed that our new strategy of ^{18}F -labeling the quinoline
8 rather than the pyrazole moiety resulted in significant metabolic stability in NHP blood.
9
10
11
12
13
14
15
16
17
18
19

20 CONCLUSION

21 In the present study, we optimized the structure of MP-10 to identify new compounds that can be ^{18}F -labeled in
22 the quinoline moiety instead of the pyrazole moiety. As a result, 20 highly potent compounds **18a-j**, **19d-j**, **20a-**
23 **b** and **21b** ($IC_{50} < 5$ nM) were identified which also displayed high selectivity for PDE10A against PDE3A/B,
24 PDE4A/B. Among these potent compounds, **18a-e**, **18g** and **20a** were evaluated as potential PET radioligands
25 for quantifying the level of PDE10A. [^{18}F]**18a**, [^{18}F]**18b**, [^{18}F]**18c**, [^{18}F]**18d**, [^{18}F]**18e**, [^{18}F]**18g**, and [^{18}F]**20a**
26 are, to our knowledge, the first MP-10 analogues successfully ^{18}F -labeled in the quinoline instead of the
27 pyrazole moiety. Rat biodistribution indicated [^{18}F]**18a**, [^{18}F]**18b**, [^{18}F]**18c**, [^{18}F]**18d**, [^{18}F]**18e**, [^{18}F]**18g**, and
28 [^{18}F]**20a** can cross the blood-brain-barrier and accumulate in the PDE10A-enriched striatum. [^{18}F]**18d** and
29 [^{18}F]**20a** proceeded to further evaluation in NHPs. The preliminary microPET imaging studies in NHPs
30 demonstrated that [^{18}F]**18d** and [^{18}F]**20a** provided very clear visualization of striatum. Although different
31 patterns of striatal clearance were observed, both tracers showed rapid clearance from non-target brain regions.
32 Compared with [^{11}C]MP-10, [^{18}F]**18d** and [^{18}F]**20a** displayed more suitable washout kinetics in NHP brain. In
33 addition, both tracers displayed favorable in vivo metabolic stability based on HPLC analysis of NHP plasma.
34 These promising preliminary results suggest that our strategy has a high probability of identifying a clinical
35 PET tracer for quantifying PDE10A in the human brain. Future NHP microPET imaging studies with [^{18}F]**18d**
36 and [^{18}F]**20a** will explore the specificity of the tracer uptake.
37
38
39
40
41
42
43
44
45
46
47
48
49
50
51
52
53
54
55
56
57
58
59
60

1 In summary, the strategy of introducing fluorine-containing group in a suitable position of the 2-
2 methylquinoline moiety of MP-10 identified new potent and selective PD10A inhibitors; this approach will help
3 guide the design of potent and selective ligands with suitable lipophilicity as candidates for treating
4 schizophrenia and other CNS diseases using PDE10A enzyme inhibition strategies. Further validation of these
5 new analogues is ongoing to determine if either is a suitable PET tracer to quantify the level of PDE10A in the
6 human brain.
7
8
9
10
11
12
13
14
15
16

17 EXPERIMENTAL SECTION

18
19 **General.** All reagents and chemicals were purchased from commercial suppliers and used without further
20 purification unless otherwise stated. All anhydrous reactions were carried out in oven-dried glassware under an
21 inert nitrogen atmosphere unless otherwise stated. When reactions involved extraction with DCM (CH₂Cl₂),
22 chloroform (CHCl₃), or ethyl acetate (EtOAc), the organic extracts were dried over anhydrous Na₂SO₄ and
23 concentrated under reduced pressure. Free bases were converted into the corresponding oxalate salt by addition
24 of oxalic acid for all final compounds. Melting points of salts were determined on the MEL-TEMP 3.0
25 apparatus and left uncorrected. ¹H NMR spectra were recorded at 400 MHz on a Varian Mercury-VX
26 spectrometer with CDCl₃ as solvents and tetramethylsilane (TMS) was used as the internal standard. Elemental
27 analyses (C, H, N) were determined by Atlantic Microlab, Inc. Synthesis of starting materials and intermediates
28 are shown in Supporting Online Information.
29
30
31
32
33
34
35
36
37
38
39
40
41
42

43 General Method for Synthesis of 18a-j, 19d-j, 20a-d, and 21b.

44
45 **4-Fluoro-2-((4-(1-methyl-4-(pyridin-4-yl)-1H-pyrazol-3-yl)phenoxy)methyl)quinoline (18a).** Sodium
46 hydride (31 mg, 1.3 mmol) was added to a solution of **16a** (251 mg, 1.00 mmol) in anhydrous DMF (20 mL) at
47 0 °C. After 30 min, **17a** (238 mg, 1.00 mmol) was added to the reaction mixture which was stirred overnight at
48 rt. The reaction mixture was then diluted with water (30 mL), extracted with DCM (3 × 60 mL), washed with 1
49 N NaOH (30 mL), dried over Na₂SO₄, filtered and concentrated under reduced pressure. The crude product was
50 purified by silica gel chromatography using MeOH: DCM (1:30, v/v) to afford **18a** as a light yellow solid (205
51 mg, 50%). ¹H NMR (CDCl₃) δ 8.48 – 8.45 (m, 2H), 8.09 – 8.07 (m, 2H), 7.80 – 7.76 (m, 1H), 7.61 – 7.57 (m,
52
53
54
55
56
57
58
59
60

2H), 7.41 – 7.38 (m, 3H), 7.18 – 7.16 (m, 2H), 7.01 – 6.99 (m, 2H), 5.37 (s, 2H), 3.96 (s, 3H). mp: 176.2 – 177.2 °C. Anal. (C₂₅H₁₉FN₄O • 2H₂C₂O₄) C, H, N: Calcd. C: 58.98, H: 3.93, N: 9.49. Found C: 58.78, H: 3.84, N: 9.26.

4-(Fluoromethyl)-2-((4-(1-methyl-4-(pyridin-4-yl)-1H-pyrazol-3-yl)phenoxy) methyl) quinoline (18b).

Triphenylphosphine (84 mg, 0.32 mmol) and DBAD (73 mg, 0.32 mmol) were added to a solution of **17a** (50 mg, 0.26 mmol) and **16b** (50 mg, 0.28 mmol) in 1,4-dioxane (2 mL) and heated at 60 °C for 18 h. The reaction mixture was quenched with 1 N NaOH (50 mL), extracted DCM (3 × 50 mL), dried over Na₂SO₄, filtered and concentrated under reduced pressure. The crude product was purified by silica gel column chromatography using MeOH: DCM (1:30, v/v) to afford **18b** as a yellow solid (55 mg, 65%). ¹H NMR (CDCl₃) δ 8.55 – 8.37 (m, 2H), 8.22 – 8.00 (m, 1H), 7.86 (d, *J* = 8.3 Hz, 1H), 7.80 – 7.70 (m, 2H), 7.63 – 7.53 (m, 2H), 7.43 – 7.33 (m, 2H), 7.20 – 7.11 (m, 2H), 7.08 – 6.93 (m, 2H), 5.94 (s, 1H), 5.83 (s, 1H), 5.39 (s, 2H), 3.95 (s, 3H). mp: 174.4 – 174.5 °C. Anal. (C₂₆H₂₁FN₄O • 2H₂C₂O₄) C, H, N: Calcd. C: 59.60, H: 4.17, N: 9.27. Found C: 59.89, H: 4.36, N: 9.15.

4-(3-Fluoropropyl)-2-((4-(1-methyl-4-(pyridin-4-yl)-1H-pyrazol-3-yl)phenoxy)methyl) quinoline (18c).

Compound **16c** was used as the starting material following the procedure described above for the preparation of **18b** to synthesize **18c** as a yellow solid (40 mg, 49%). ¹H NMR (CDCl₃) δ 8.45 (d, *J* = 5.0 Hz, 2H), 8.05 (m, 2H), 7.71 (t, *J* = 7.5 Hz, 1H), 7.55 (dd, *J* = 14.5, 7.1 Hz, 2H), 7.37 (d, *J* = 8.4 Hz, 2H), 7.24 (s, 1H), 7.14 (d, *J* = 5.0 Hz, 2H), 7.00 (d, *J* = 8.3 Hz, 2H), 5.35 (s, 2H), 4.56 (t, *J* = 5.6 Hz, 1H), 4.44 (t, *J* = 5.5 Hz, 1H), 3.95 (s, 3H), 3.22 (t, *J* = 7.7 Hz, 2H), 2.25 – 2.05 (m, 2H). mp: 125.3 – 125.5 °C. Anal. (C₂₈H₂₅FN₄O • 2H₂C₂O₄) C, H, N: Calcd. C: 60.76, H: 4.62, N: 8.86. Found C: 60.86, H: 4.51, N: 8.63.

4-(2-Fluoroethoxy)-2-((4-(1-methyl-4-(pyridin-4-yl)-1H-pyrazol-3-yl)phenoxy)methyl) quinoline (18d).

Compound **16d** was used as the starting material following the procedure described above for the preparation of **18b** to synthesize **18d** as a white solid (82 mg, 67%). ¹H-NMR (CDCl₃): δ 8.46 (s, 2H), 8.24 (d, *J* = 7.5 Hz, 1H), 7.99 (d, *J* = 6.7 Hz, 1H), 7.71 (s, 1H), 7.64 – 7.46 (m, *J* = 22.3 Hz, 2H), 7.38 (d, *J* = 6.6 Hz, 2H), 7.15 (s, 2H), 7.00 (s, 3H), 5.33 (s, 2H), 4.89 (d, *J* = 47.9 Hz, 2H), 4.43 (d, *J* = 26.9 Hz, 2H), 3.95 (s, 3H). mp: 126.2-

126.3 °C. Anal. (C₂₇H₂₃FN₄O₂ • 2H₂C₂O₄) C, H, N: Calcd. C: 58.68, H: 4.29, N: 8.83. Found C: 58.98, H: 4.19, N: 8.91.

4-((2-Fluoroethoxy)methyl)-2-((4-(1-methyl-4-(pyridin-4-yl)-1H-pyrazol-3-yl)phenoxy) methyl)quinoline (18e). Compound **16h** was used as the starting material following the procedure described above for the preparation of **18b** to synthesize **18e** as a white solid (69 mg, 69%). ¹H-NMR (CDCl₃): δ 8.45 (dd, *J* = 4.6, 1.5 Hz, 2H), 8.09 (d, *J* = 8.5 Hz, 1H), 7.98 (d, *J* = 8.4 Hz, 1H), 7.78 – 7.67 (m, 2H), 7.61 – 7.50 (m, 2H), 7.38 (d, *J* = 8.8 Hz, 2H), 7.14 (dd, *J* = 4.6, 1.6 Hz, 2H), 7.01 (d, *J* = 8.8 Hz, 2H), 5.37 (s, 2H), 5.06 (s, 2H), 4.71 – 4.61 (m, 1H), 4.58 – 4.49 (m, 1H), 3.94 (s, 3H), 3.87 – 3.81 (m, 1H), 3.80 – 3.74 (m, 1H). mp: 126.8-127.4 °C. Anal. (C₂₈H₂₅FN₄O₂ • 2H₂C₂O₄) C, H, N. Calcd. C: 59.26, H: 4.51, N: 8.64. Found C: 58.09, H: 4.77, N: 8.88.

4-(2-(2-Fluoroethoxy)ethoxy)-2-((4-(1-methyl-4-(pyridin-4-yl)-1H-pyrazol-3-yl)phenoxy) methyl) quinoline (18f). Compound **16e** was used as the starting material following the procedure described above for the preparation of **18b** to synthesize **18f** as a white solid (64 mg, 68%). ¹H NMR (CDCl₃) δ 8.50 – 8.42 (m, 2H), 8.20 (d, *J* = 8.3 Hz, 1H), 7.98 (d, *J* = 8.4 Hz, 1H), 7.70 (t, *J* = 7.6 Hz, 1H), 7.56 (s, 1H), 7.49 (t, *J* = 7.5 Hz, 1H), 7.38 (d, *J* = 8.6 Hz, 2H), 7.15 (d, *J* = 5.8 Hz, 2H), 7.04 – 6.95 (m, 3H), 5.33 (s, 2H), 4.68 – 4.61 (m, 1H), 4.58 – 4.50 (m, 1H), 4.40 – 4.32 (m, 2H), 4.06 – 3.99 (m, 2H), 3.95 (s, 3H), 3.92 – 3.86 (m, 1H), 3.85 – 3.79 (m, 1H). mp: 170.1-170.3 °C. Anal. (C₂₉H₂₇FN₄O₃ • 2H₂C₂O₄) C, H, N: C: 58.41, H: 4.60, N: 8.26. Found C: 58.70, H: 4.81, N: 8.45.

4-(2-(2-(2-Fluoroethoxy)ethoxy)ethoxy)-2-((4-(1-methyl-4-(pyridin-4-yl)-1H-pyrazol-3-yl)phenoxy)-methyl) quinoline (18g). Compound **16f** was used as the starting material following the procedure described above for the preparation of **18b** to synthesize **18g** as a white solid (55 mg, 63%). ¹H-NMR (CDCl₃): δ 8.47 (d, *J* = 5.8 Hz, 2H), 8.22 (d, *J* = 8.3 Hz, 1H), 7.98 (d, *J* = 8.4 Hz, 1H), 7.70 (t, *J* = 7.6 Hz, 1H), 7.57 (s, 1H), 7.49 (t, *J* = 7.6 Hz, 1H), 7.39 (d, *J* = 8.6 Hz, 2H), 7.16 (d, *J* = 5.9 Hz, 2H), 7.07 – 6.96 (m, 3H), 5.33 (s, 2H), 4.63 – 4.56 (m, 1H), 4.51 – 4.44 (m, 1H), 4.41 – 4.31 (m, 2H), 4.01 (t, *J* = 4.6 Hz, 2H), 3.96 (s, 3H), 3.83 – 3.71 (m, 6H). mp: 166.0-166.2 °C. Anal. (C₃₁H₃₁FN₄O₄ • 2H₂C₂O₄) C, H, N: Calcd. C: 58.17, H: 4.88, N: 7.75. Found C: 58.33, H: 4.98, N: 7.94.

4-(2-(2-(2-(2-Fluoroethoxy)ethoxy)ethoxy)ethoxy)-2-((4-(1-methyl-4-(pyridin-4-yl)-1H-pyrazol-3-yl)phenoxy) methyl)quinoline (18h). Compound **16g** was used as the starting material following the procedure described above for the preparation of **18b** to synthesize **18h** as a white solid (48 mg, 59%). ¹H-NMR (CDCl₃): δ 8.46 (d, *J* = 5.9 Hz, 2H), 8.21 (d, *J* = 8.3 Hz, 1H), 7.98 (d, *J* = 8.4 Hz, 1H), 7.69 (t, *J* = 7.6 Hz, 1H), 7.56 (s, 1H), 7.48 (t, *J* = 7.6 Hz, 1H), 7.38 (d, *J* = 8.7 Hz, 2H), 7.15 (d, *J* = 5.9 Hz, 2H), 7.05 – 6.95 (m, 3H), 5.32 (s, 2H), 4.61 – 4.55 (m, 1H), 4.49 – 4.42 (m, 1H), 4.35 (t, *J* = 4.6 Hz, 2H), 4.00 (t, *J* = 4.6 Hz, 2H), 3.95 (s, 3H), 3.82 – 3.62 (m, 10H). mp: 128.4-129.0 °C. Anal. (C₃₃H₃₅FN₄O₅ • 2H₂C₂O₄) C, H, N: Calcd. C: 57.96, H: 5.13, N: 7.31. Found C: 58.06, H: 5.31, N: 7.50.

N-(2-Fluoroethyl)-2-((4-(1-methyl-4-(pyridin-4-yl)-1H-pyrazol-3-yl)phenoxy) methyl) quinolin-4-amine (18i). Compound **16i** was used as the starting material following the procedure described above for the preparation of **18b**, then used TFA for deprotection to afford **18i** as a light yellow solid (42 mg, 63%). ¹H-NMR (CDCl₃): δ 8.47 (d, *J* = 4.0 Hz, 2H), 7.99 (d, *J* = 4.4 Hz, 1H), 7.86 – 7.83 (m, 1H), 7.64-7.61 (m, 1H), 7.57 (s, 1H), 7.42-7.37 (m, 3H), 7.17 – 7.15 (m, 2H), 7.03-7.01 (m, 2H), 6.63 (s, 1H), 5.33 (s, 2H), 4.82 – 4.79 (m, 1H), 4.70 – 4.67 (m, 1H), 3.96 (s, 3H), 3.76 – 3.69 (m, 2H). mp: 210.6 – 210.7 °C. Anal. (C₂₇H₂₄FN₅O • 2H₂C₂O₄) C, H, N: Calcd. C: 58.77, H: 4.45, N: 11.05. Found C: 58.98, H: 4.34, N: 11.23.

4-(4-(2-Fluoroethyl)-1H-1,2,3-triazol-1-yl)-2-((4-(1-methyl-4-(pyridin-4-yl)-1H-pyrazol-3-yl)phenoxy)methyl)quinoline (18j). Compound **16j** was used as the starting material following the procedure described above for the preparation of **18b** to synthesize **18j** as a light yellow solid (59 mg, 64%). ¹H NMR (CDCl₃) δ 8.52 – 8.44 (m, 2H), 8.23 – 8.17 (m, 1H), 8.02 – 7.96 (m, 1H), 7.96 – 7.93 (m, 1H), 7.88 – 7.80 (m, 2H), 7.65-7.63 (m, 1H), 7.57 (s, 1H), 7.44 – 7.37 (m, 2H), 7.19 – 7.13 (m, 2H), 7.07 – 6.99 (m, 2H), 5.45 (s, 2H), 4.89 (t, *J* = 5.9 Hz, 1H), 4.77 (t, *J* = 5.9 Hz, 1H), 3.97 (s, 3H), 3.35 (t, *J* = 5.9 Hz, 1H), 3.28 (t, *J* = 5.9 Hz, 1H). mp: 214.2-214.6°C. Anal. (C₂₉H₂₄FN₇O • 2H₂C₂O₄) C, H, N: Calcd. C: 57.81, H: 4.12, N: 14.30. Found C: 57.97, H: 4.01, N: 14.42.

4-(2-Fluoroethoxy)-2-((4-(1-methyl-4-(pyridin-4-yl)-1H-pyrazol-5-yl)phenoxy) methyl) quinoline (19d). Compound **16d** with **17b** (in place of **17a**) were used as the starting materials following the procedure described above for the preparation of **18b** to synthesize **19d** as a white solid (86 mg, 70%). ¹H-NMR (CDCl₃): δ 8.38 (d,

1 $J = 2.4$ Hz, 2H), 8.29 – 8.27 (m, 1H), 8.03-8.01 (m, 1H), 7.82 (s, 1H), 7.75 (m, 1H), 7.57-7.53 (m, 1H), 7.26 –
2 7.22 (m, 3H), 7.16 – 7.14 (m, 2H), 7.06 – 7.03 (m, 3H), 5.38 (s, 2H), 5.00 (s, 1H), 4.86 (s, 1H), 4.55 (s, 1H),
3 4.45 (s, 1H), 3.75 (s, 3H). mp: 189.1 – 189.3 °C. Anal. ($C_{27}H_{23}FN_4O_2 \cdot 2H_2C_2O_4$) C, H, N: Calcd. C: 58.68, H:
4 4.29, N: 8.83. Found C: 58.58, H: 4.49, N: 9.01.

5
6
7
8
9
10 **4-((2-Fluoroethoxy)methyl)-2-((4-(1-methyl-4-(pyridin-4-yl)-1H-pyrazol-5-yl)phenoxy) methyl)quinoline**
11 **(19e)**. Compound **16h** with **17b** (in place of **17a**) were used as the starting materials following the procedure
12 described above for the preparation of **18b** to synthesize **19e** as a white solid (62 mg, 69%). 1H NMR ($CDCl_3$) δ
13 8.39 – 8.38 (m, 2H), 8.14 – 8.12 (m, 1H), 8.02 – 8.00 (m, 1H), 7.82 (s, 2H), 7.77 – 7.74 (m, 1H), 7.62 – 7.58
14 (m, 1H), 7.26 – 7.23 (m, 2H), 7.18 – 7.16 (m, 2H), 7.05 – 7.04 (m, 2H), 5.43 (s, 2H), 5.12 (s, 2H), 4.73 – 4.71
15 (m, 1H), 4.61 – 4.59 (m, 1H), 3.94 – 3.92 (m, 1H), 3.87 – 3.85 (m, 1H), 3.75 (s, 3H). mp: 121.3 – 121.8 °C.
16
17
18
19
20
21
22
23
24 Anal. ($C_{28}H_{25}FN_4O_2 \cdot 2H_2C_2O_4$) C, H, N: Calcd. C: 59.26, H: 4.51, N: 8.64. Found C: 59.45, H: 4.31, N: 8.51.

25
26 **4-(2-(2-Fluoroethoxy)ethoxy)-2-((4-(1-methyl-4-(pyridin-4-yl)-1H-pyrazol-5-yl)phenoxy) methyl)**
27 **quinoline (19f)**. Compound **16e** with **17b** (in place of **17a**) were used as the starting materials following the
28 procedure described above for the preparation of **18b** to synthesize **19f** as a white solid (58 mg, 62%). 1H -NMR
29 ($CDCl_3$): δ 8.39-8.38 (m, 2H), 8.24 (d, $J = 4.0$ Hz, 1H), 8.01 (d, $J = 4.3$ Hz, 1H), 7.81 (s, 1H), 7.73 (m, 1H), 7.52
30 (m, 1H), 7.26 – 7.04 (m, 7H), 5.38 (s, 2H), 4.69 (m, 1H), 4.53 (m, 1H), 4.41 (m, 2H), 4.06 (m, 2H), 3.94 – 3.93
31 (m, 1H), 3.85-3.83 (m, 1H), 3.75 (m, 3H). mp: 109.6 – 109.7 °C. Anal. ($C_{29}H_{27}FN_4O_3 \cdot 2H_2C_2O_4$) C, H, N:
32 Calcd. C: 58.41, H: 4.60, N: 8.26. Found C: 58.63, H: 4.79, N: 8.45.

33
34
35
36
37
38
39
40
41
42
43 **4-(2-(2-(2-Fluoroethoxy)ethoxy)ethoxy)-2-((4-(1-methyl-4-(pyridin-4-yl)-1H-pyrazol-5-yl)phenoxy)**
44 **methyl)quinoline (19g)**. Compound **16f** with **17b** (in place of **17a**) were used as the starting materials
45 following the procedure described above for the preparation of **18b** to synthesize **19g** as a white solid (52 mg,
46 60%). 1H -NMR ($CDCl_3$): δ 8.39 – 8.38 (m, 2H), 8.25 (d, $J = 4.0$ Hz, 1H), 8.01 (d, $J = 4.3$ Hz, 1H), 7.82 (s, 1H),
47 7.75 – 7.70 (m, 1H), 7.54 – 7.49 (m, 1H), 7.26-7.03 (m, 7H), 5.38 (s, 2H), 4.63 (m, 1H), 4.47 – 4.40 (m, 3H),
48 4.06 – 4.04 (m, 2H), 3.82-3.72 (m, 9H). mp: 82.0 – 82.1 °C. Anal. ($C_{31}H_{31}FN_4O_4 \cdot 2H_2C_2O_4$) C, H, N: Calcd. C:
49 58.17, H: 4.88, N: 7.75. Found C: 58.35, H: 4.99, N: 7.62.

50
51
52
53
54
55
56
57
58
59
60 **(2-(2-(2-(2-Fluoroethoxy)ethoxy)ethoxy)ethoxy)-2-((4-(1-methyl-4-(pyridin-4-yl)-1H-pyrazol-5-**

yl)phenoxy) methyl)quinoline (19h). Compound **16g** with **17b** (in place of **17a**) were used as the starting materials following the procedure described above for the preparation of **18b** to synthesize **19h** as a white solid (46 mg, 57%). ¹H-NMR (CDCl₃): δ 8.39 – 8.37 (m, 2H), 8.24 (d, *J* = 4.0 Hz, 1H), 8.00 (d, *J* = 4.3 Hz, 1H), 7.81 (s, 1H), 7.74 – 7.70 (m, 1H), 7.53 – 7.49 (m, 1H), 7.24 – 7.22 (m, 2H), 7.16 – 7.13 (m, 2H), 7.05 – 7.03 (m, 3H), 5.37 (s, 2H), 4.50 – 4.58 (m, 1H), 4.48-4.46 (m, 1H), 4.40 – 4.38 (m, 2H), 4.40 – 4.38 (m, 2H), 3.81 – 3.67 (m, 13H). mp: 108.8 – 108.9 °C. Anal. (C₃₃H₃₅FN₄O₅ • 2H₂C₂O₄) C, H, N: Calcd. C: 57.96, H: 5.13, N: 7.31. Found C: 57.71, H: 5.33, N: 7.47.

N-(2-Fluoroethyl)-2-((4-(1-methyl-4-(pyridin-4-yl)-1H-pyrazol-5-yl)phenoxy)methyl) quinolin-4-amine (19i). Compound **16i** with **17b** (in place of **17a**) were used as the starting materials following the procedure described above for the preparation of **18b**, then deprotection with TFA afforded **19i** as a yellow solid (40 mg, 60%). ¹H-NMR (CDCl₃): δ 8.37 (d, *J* = 3.0 Hz, 2H), 7.99 (d, *J* = 4.2 Hz, 1H), 7.81 – 7.77 (m, 2H), 7.71 – 7.67 (m, 1H), 7.50-7.46 (m, 1H), 7.23 – 7.21 (m, 2H), 7.15 – 7.13 (m, 2H), 7.05 – 7.03 (m, 2H), 6.75 (s, 1H), 5.33 (s, 2H), 4.82 – 4.79 (m, 1H), 4.70 – 4.67 (m, 1H), 3.76-3.69 (m, 5H). mp: 206.5 – 206.7 °C. Anal. (C₂₇H₂₄FN₅O • 2H₂C₂O₄) C, H, N: Calcd. C: 58.77, H: 4.45, N: 11.05. Found C: 58.53, H: 4.71, N: 11.22.

4-(4-(2-Fluoroethyl)-1H-1,2,3-triazol-1-yl)-2-((4-(1-methyl-4-(pyridin-4-yl)-1H-pyrazol-5-yl)phenoxy)methyl)quinoline (19j). Compound **16j** with **17b** (in place of **17a**) were used as the starting materials following the procedure described above for the preparation of **18b** to synthesize **19j** as a light yellow solid (62 mg, 67%). ¹H NMR (CDCl₃) δ 8.38 – 8.36 (m, 2H), 8.22 – 8.20 (m, 1H), 7.99 – 7.97 (m, 2H), 7.87 – 7.84 (m, 2H), 7.80 (s, 1H), 7.68 – 7.64 (m, 1H), 7.26 – 7.23 (m, 2H), 7.16 – 7.14 (m, 2H), 7.04 – 7.02 (m, 2H), 5.48 (s, 2H), 4.89 (t, *J* = 5.8 Hz, 1H), 4.77 (t, *J* = 5.8 Hz, 1H), 3.74 (s, 3H), 3.35 (t, *J* = 5.8 Hz, 1H), 3.28 (t, *J* = 5.8 Hz, 1H). mp: 172.3-172.7°C. Anal. (C₂₉H₂₄FN₇O • 2H₂C₂O₄) C, H, N: Calcd. C: 57.81, H: 4.12, N: 14.30. Found C: 58.01, H: 4.02, N: 14.52.

3-(2-Fluoroethoxy)-2-((4-(1-methyl-4-(pyridin-4-yl)-1H-pyrazol-3-yl)phenoxy)methyl) quinoline (20a). Compound **16k** was used as the starting material following the procedure described above for the preparation of **18b** to synthesize **20a** as a light yellow solid (60 mg, 67%). ¹H-NMR (CDCl₃): δ 8.44 (d, *J* = 4.9 Hz, 2H), 8.07 (d, *J* = 8.3 Hz, 1H), 7.71 (d, *J* = 8.1 Hz, 1H), 7.60 – 7.46 (m, 3H), 7.43 (s, 1H), 7.36 (d, *J* = 8.5 Hz, 2H), 7.19 –

7.11 (m, 2H), 7.05 (d, $J = 8.5$ Hz, 2H), 5.43 (s, 2H), 4.85 (d, $J = 3.8$ Hz, 1H), 4.73 (d, $J = 3.9$ Hz, 1H), 4.40 (d, $J = 3.7$ Hz, 1H), 4.33 (d, $J = 3.6$ Hz, 1H), 3.96 (s, 3H). mp: 191.4 - 191.7 °C. Anal. ($C_{27}H_{23}FN_4O_2 \cdot 2H_2C_2O_4$) C, H, N: Calcd. C: 58.68, H: 4.29, N: 8.83. Found C: 58.73, H: 4.48, N: 8.99.

6-Fluoro-2-((4-(1-methyl-4-(pyridin-4-yl)-1H-pyrazol-3-yl) phenoxy) methyl) quinoline (20b). Compound

16l was used as the starting material following the procedure described above for the preparation of **18b** to synthesize **20b** as a white solid (56 mg, 69%). 1H NMR ($CDCl_3$) δ 8.52 – 8.42 (m, 2H), 8.14 (d, $J = 8.6$ Hz, 1H), 8.07 (dd, $J = 9.3, 5.3$ Hz, 1H), 7.70 (d, $J = 8.7$ Hz, 1H), 7.57 (s, 1H), 7.55 – 7.42 (m, 2H), 7.43 – 7.35 (m, 2H), 7.20 – 7.12 (m, 2H), 7.04 – 6.97 (m, 2H), 5.38 (s, 2H), 3.97 (s, 3H). mp: 213.3 – 213.5 °C. Anal. ($C_{25}H_{19}FN_4O \cdot 2H_2C_2O_4$) C, H, N: Calcd. C: 58.98, H: 3.93, N: 9.49. Found C: 59.09, H: 3.71, N: 9.57.

6-(Fluoromethyl)-2-((4-(1-methyl-4-(pyridin-4-yl)-1H-pyrazol-3-yl)phenoxy) methyl) quinoline (20c).

Compound **16m** was used as the starting material following the procedure described above for the preparation of **18b** to synthesize **20c** as a light solid (50 mg, 61%). 1H NMR ($CDCl_3$) δ 8.51 – 8.34 (m, 2H), 8.16 (d, $J = 8.5$ Hz, 1H), 8.07 (d, $J = 8.7$ Hz, 1H), 7.79 (t, $J = 2.2$ Hz, 1H), 7.74 – 7.64 (m, 2H), 7.53 (s, 1H), 7.43 – 7.32 (m, 2H), 7.22 – 7.09 (m, 2H), 7.02 – 6.90 (m, 2H), 5.59 (s, 1H), 5.47 (s, 1H), 5.37 (s, 2H), 3.96 (s, 3H). mp: 220.7 – 220.8 °C. Anal. ($C_{26}H_{21}FN_4O \cdot 2H_2C_2O_4$) C, H, N: Calcd. C: 59.60, H: 4.17, N: 9.27. Found C: 59.78, H: 4.29, N: 9.15.

6-(2-Fluoroethoxy)-2-((4-(1-methyl-4-(pyridin-4-yl)-1H-pyrazol-3-yl)phenoxy) methyl) quinoline (20d).

Compound **16n** was used as the starting material following the procedure described above for the preparation of **18a** to synthesize **20d** as a light yellow solid (290 mg, 61%). 1H -NMR ($CDCl_3$): δ 8.48 – 8.46 (m, 2H), 8.07 (d, $J = 8.5$ Hz, 1H), 7.99 (d, $J = 9.2$ Hz, 1H), 7.64-7.62 (m, 1H), 7.57 (s, 1H), 7.43-7.37 (m, 3H), 7.16 – 7.14 (m, 2H), 7.09 – 7.08 (m, 1H), 7.01 – 6.99 (m, 2H), 5.35 (s, 2H), 4.90 – 4.88 (m, 1H), 4.78 – 4.76 (m, 1H), 4.38 – 4.36 (m, 1H), 4.31 – 4.29 (m, 1H), 3.96 (s, 3H). mp: 228.8 – 228.9 °C. Anal. ($C_{27}H_{23}FN_4O_2 \cdot 2H_2C_2O_4$) C, H, N: Calcd. C: 58.68, H: 4.29, N: 8.83. Found C: 58.83, H: 4.56, N: 8.73.

6-Fluoro-2-((4-(1-methyl-4-(pyridin-4-yl)-1H-pyrazol-5-yl)phenoxy)methyl)quinoline (21b). 6-

Fluoroquinolin-2-yl)methanol (**16l**) with **17b** (in place of **17a**) were used as the starting materials following the procedure described above for the preparation of **18b** to synthesize **21b** as a white solid (53 mg, 65%) 1H NMR

(CDCl₃) δ 8.39 (dd, $J = 4.7, 1.4$ Hz, 2H), 8.19 (d, $J = 8.5$ Hz, 1H), 8.09 (dd, $J = 9.2, 5.3$ Hz, 1H), 7.82 (s, 1H), 7.74 (d, $J = 8.5$ Hz, 1H), 7.58 – 7.42 (m, 2H), 7.30 – 7.21 (m, 2H), 7.15 (d, $J = 8.8$ Hz, 2H), 7.07 – 7.00 (m, 2H), 5.42 (s, 2H), 3.75 (s, 3H). mp: 220.8 – 220.9 °C. Anal. (C₂₅H₁₉FN₄O • 2H₂C₂O₄) C, H, N: Calcd. C: 58.98, H: 3.93, N: 9.49. Found C: 58.85, H: 4.11, N: 9.68.

General Radiochemistry. We used both one- and two-step approaches for radiolabeling; methods for each are described below. [¹⁸F]Fluoride is produced by a ¹⁸O(p, n)¹⁸F reaction through proton irradiation of enriched ¹⁸O water (95%) using Washington University's RDS-111 cyclotron (Siemens/CTI Molecular Imaging, Knoxville, TN, USA). [¹⁸F]Fluoride is first passed through an ion-exchange resin then eluted with 0.02 M potassium carbonate (K₂CO₃) solution.

Following the one- or two-step incorporation of [¹⁸F]Fluoride, the reaction mixtures were purified using a semi-preparative HPLC system which contains a 5-mL injection loop, a semi-preparative column, UV detector at 254 nm, and an in-line radioactivity detector which is used to identify the desired product for collection in a vial containing 50 mL sterile water. The diluted eluent was trapped on a C-18 Plus Sep-Pak cartridge, which was then rinsed with 10 mL sterile water; the product was eluted with 0.6 mL ethanol followed by 5.4 mL saline. After the diluted radiotracer was sterile-filtered through a 0.22 μ m syringe filter into a sterile glass vial, and an aliquot was removed for QC testing. The total synthesis time was ~ 2 h for one-step labeling and ~ 3 h for two-step labeling. Quality control was conducted on an analytical HPLC system with UV detection at 254 nm. The radioactive dose was authenticated by co-injection with the nonradioactive reference compound.

Synthesis of [¹⁸F]18a: a one-step general procedure for radiosynthesis of [¹⁸F]18a, [¹⁸F]18b, [¹⁸F]18c, [¹⁸F]18e, and [¹⁸F]18g

4-(Fluoro-¹⁸F)-2-((4-(1-methyl-4-(pyridin-4-yl)-1H-pyrazol-3-yl)phenoxy)methyl)quinoline ([¹⁸F]18a). A sample of ~7.40 GBq [¹⁸F]/fluoride/K₂CO₃ was added to a reaction vessel containing Kryptofix [222] (6.5–7.0 mg), and dried by azeotropic distillation at 110 °C using MeCN (3 × 1 mL) under a gentle flow of nitrogen. 1.0 – 3.0 mg of the bromide precursor **23a** dissolved in DMSO (200 - 300 μ L) was then transferred to the reaction vessel which was capped, vortexed, and heated in an oil bath at 170 - 175 °C for 20 min. After the heat source

1 was removed, the reaction mixture was diluted with 3.0 mL of HPLC mobile phase and purified using an
2 Agilent SB-C18 column with MeCN/0.1 M ammonium formate buffer pH 4.5 (48/52, v/v) as the mobile phase
3 at a flow rate of 4.0 mL/min; the retention time for the desired product was 19 - 21 min. QC was conducted on a
4 Grace Alltima C-18 column (250 mm × 4.6 mm), with a mobile phase of MeCN/0.1 M ammonium formate
5 buffer pH 4.5 (62/38, v/v) at 1.8 mL/min. The retention time of [¹⁸F]**18a** was 5.1 min. The radiochemical purity
6 was >99%, the yield was 4.2-4.8% (decay-corrected) and - SA was > 74 GBq/μmol (decay-corrected to EOS).

7
8
9
10
11
12
13
14 **4-((Fluoro-¹⁸F)methyl)-2-((4-(1-methyl-4-(pyridin-4-yl)-1H-pyrazol-3-yl)phenoxy) methyl) quinoline**
15 (**[¹⁸F]18b**). The chloride precursor **23b** was used for the one-step radiolabeling of [¹⁸F]**18b** as described above
16 for [¹⁸F]**18a**. The reaction temperature was 105 - 110 °C for 20 min. The reaction mixture was purified using an
17 Agilent SB-C18 column with a mobile phase of MeCN/0.1 M ammonium formate buffer pH 4.5 (40/60, v/v) at
18 4.0 mL/min; the retention time for the desired product was 24 - 26 min. QC was performed using a Phenomenex
19 Prodigy C-18 column (250 mm × 4.6 mm) with a mobile phase of MeCN/0.1 M ammonium formate buffer pH
20 4.5 (62/38, v/v) at 1.5 mL/min. The retention time of [¹⁸F]**18b** was 4.9 min. The radiochemical purity was >
21 99%, the chemical purity was > 95%, the yield was 1.1-1.5% (decay-corrected) and the SA was > 74 GBq/μmol
22 (decay-corrected to EOS).

23
24
25
26
27
28
29
30
31
32
33
34
35
36 **4-(3-(Fluoro-¹⁸F)propyl)-2-((4-(1-methyl-4-(pyridin-4-yl)-1H-pyrazol-3-yl)phenoxy)methyl) quinoline**
37 (**[¹⁸F]18c**). The mesylate precursor **23c** was used for the one-step radiolabeling of [¹⁸F]**18c** as described above
38 for [¹⁸F]**18a**. The reaction temperature was 75 - 80 °C for 20 min. The reaction mixture was purified using an
39 Agilent SB-C18 column with a mobile phase of MeCN/0.1 M ammonium formate buffer pH 4.5 (50/50, v/v) at
40 4.0 mL/min; the retention time for the desired product was 17 - 18 min. QC was performed using an Agilent
41 SB- C18 column (250 mm × 4.6 mm) with a mobile phase of MeCN/0.1 M ammonium formate buffer pH 4.5
42 (65/35, v/v) at 1.5 mL/min. The retention time of [¹⁸F]**18c** was 4.9 min. The radiochemical purity was > 99%,
43 the yield was 10.1-12.2% (decay-corrected) and the SA was > 74 GBq/μmol (decay-corrected to EOS).

44
45
46
47
48
49
50
51
52
53
54
55 **4-((2-(Fluoro-¹⁸F)ethoxy)methyl)-2-((4-(1-methyl-4-(pyridin-4-yl)-1H-pyrazol-3-yl) phenoxy) methyl)-**
56 **quinoline** (**[¹⁸F]18e**). The mesylate precursor **23e** was used for the one-step radiolabeling of [¹⁸F]**18e** as
57 described above for [¹⁸F]**18a**. The reaction temperature was 85 - 90 °C for 15 min. The reaction mixture was
58
59
60

1 purified using an Agilent SB-C18 column with a mobile phase of MeCN/0.1 M ammonium formate buffer pH
2 4.5 (40/60, v/v) at 4.0 mL/min; the retention time was 21.8 min. QC was performed using a Grace Alltima- C18
3 column (250 mm × 4.6 mm) with a mobile phase of MeCN/0.1 M ammonium formate buffer pH 4.5 (62/38,
4 v/v) at 1.8 mL/min. The retention time of [¹⁸F]**18e** was 4.4 min. The radiochemical purity was >99%, the
5 chemical purity was > 95%, the yield was 15-18% (decay-corrected) and the SA was > 74 GBq/μmol (decay
6 corrected to EOS).
7
8
9

10 **2-(2-(2-((2-((4-(1-Methyl-4-(pyridin-4-yl)-1H-pyrazol-3-yl)phenoxy)methyl)quinolin-4-yl)oxy)ethoxy)-**
11 **ethoxy)ethyl hypofluorite-¹⁸F ([¹⁸F]**18g**).** The tosylate precursor **23g** was used for the one-step radiolabeling of
12 [¹⁸F]**18g** as described above for [¹⁸F]**18a**. The reaction temperature was 95 - 100 °C for 15 min. The reaction
13 mixture was purified using an Agilent SB-C18 column with a mobile phase of MeCN/0.1 M ammonium
14 formate buffer pH 6.5 (50/50, v/v) at 3.5 mL/min; the retention time for the desired product was 13 min. QC
15 was performed using an Agilent SB-C18 column (250 mm × 4.6 mm) with a mobile phase of MeCN/0.1 M
16 ammonium formate buffer pH 6.5 (56/44, v/v) at 1.5 mL/min. The retention time of [¹⁸F]**18g** was 4.9 min. The
17 radiochemical purity was > 99%, the chemical purity was > 95%, the yield was 27-30% (decay-corrected) and
18 the SA was > 74 GBq/μmol (decay-corrected to EOS).
19
20
21
22
23
24
25
26
27
28
29
30
31
32
33
34
35

36 **Synthesis of [¹⁸F]**20a**: a two-step general procedure for radiosynthesis [¹⁸F]**20a** and [¹⁸F]**18d****

37
38 **3-((2-Fluoro-¹⁸F)ethoxy)-2-((4-(1-methyl-4-(pyridin-4-yl)-1H-pyrazol-3-yl)phenoxy)methyl) quinoline**
39 **([¹⁸F]**20a**).** A sample of ~7.40 GBq [¹⁸F]/fluoride/K₂CO₃ was added to a reaction vessel containing Kryptofix
40 [222] (7.0 – 8.0 mg). The syringe was washed with 2 × 0.4 mL ethanol, evaporated and dried by azeotropic
41 distillation at 110 °C using MeCN (3 × 1 mL) under a gentle flow of N₂ gas. After all water was removed, 5.0-
42 5.5 mg of the di-tosylate **33** was dissolved in MeCN (200 μL) mixed, then transferred into the reaction vessel
43 containing [¹⁸F]fluoride/Kryptofix[222]/K₂CO₃ which was capped, mixed, and heated in an oil bath to 100 °C
44 for 15 min. After the heat source was removed, the reaction mixture was diluted with 3.0 mL of HPLC mobile
45 phase and passed through an alumina Neutral Sep-Pak Plus cartridge. The reaction mixture was then purified
46 with an Agilent SB-C18 column (250 mm × 10 mm) with a mobile phase of MeCN/0.1 M ammonium formate
47 buffer pH 6.5 (50/50, v/v) at 4.0 mL/min; the retention time of the [¹⁸F]fluoroethyl tosylate product was 9.5-10
48
49
50
51
52
53
54
55
56
57
58
59
60

1 min. The retention time of the precursor was 23-24 min. The product was diluted with 50 mL sterile water then
2 trapped on a C-18 Sep-Pak Plus cartridge. The trapped product was eluted with diethyl ether (2.5 mL).
3

4
5 The eluted solution formed two phases, the top organic phase was removed and reserved, and the bottom
6 aqueous phase was extracted with 1 mL of ether. The ether extracts were combined and passed through two
7 Sep-Pak Plus dry cartridges in series into a reaction vessel; the ether was evaporated under a stream of nitrogen.
8
9 1 - 2 mg of phenol precursor **24a** was then dissolved in 200 μ L DMSO and transferred to a vial containing 2.0
10 mg Cs_2CO_3 and vortexed for 1 min; this saturated Cs_2CO_3 solution was added to the reaction vessel which was
11 capped, mixed, and heated in an oil bath at 85-90 $^\circ\text{C}$ for 15 min. The reaction mixture was diluted with 3.0 mL
12 HPLC mobile phase and purified using an Agilent SB C-18 column with a mobile phase of MeCN/0.1 M
13 ammonium formate buffer pH 4.5 (40/60, v/v) at 4.0 mL/min; the retention time was 21.4 min. QC was
14 performed using an Agilent Zorbax, SB-C18 column (250 mm \times 4.6 mm) with a mobile phase of MeCN/0.1 M
15 ammonium formate buffer pH 4.5 (56/44, v/v) at 1.5 mL/min. The retention time of [^{18}F]**20a** was 4.8 min. The
16 radiochemical purity was > 99%, the chemical purity was > 95%, the yield was 65-72% (decay-corrected) and
17 the SA was > 74 GBq/ μ mol (decay-corrected to EOS).
18
19
20
21
22
23
24
25
26
27
28
29
30
31
32

33 **4-((2-Fluoro- ^{18}F)ethoxy)-2-((4-(1-methyl-4-(pyridin-4-yl)-1H-pyrazol-3-yl)phenoxy)methyl) quinoline**
34 (**[^{18}F]**18d**). The phenol precursor **23d** was used for the two-step labeling of [^{18}F]**18d** as described above for
35 [^{18}F]**20a**. The reaction temperature was 95-100 $^\circ\text{C}$ for 15 min. The reaction mixture was purified on an Agilent
36 SB-C18 column with a mobile phase of MeCN/0.1 M ammonium formate buffer pH 4.5 (45/55, v/v) at 4.0
37 mL/min; the retention time was 16.2 min. QC was performed using an Agilent Zorbax, SB-C18 column (250
38 mm \times 4.6 mm) with a mobile phase of MeCN/0.1 M ammonium formate buffer pH 4.5 (50/50, v/v) at 1.4
39 mL/min. The retention time of [^{18}F]**18d** was 7.5 min. The radiochemical purity was >99%, the chemical purity
40 was 95%, the yield was 30-35% (decay-corrected) and the SA was > 74 GBq/ μ mol (decay-corrected to EOS).
41
42
43
44
45
46
47
48
49
50
51**

52 **In vitro assay.** The PDE10A in vitro screening assay followed our previously published procedures.³⁵ PDE
53 activity was measured using the Phosphodiesterase [^3H]cAMP Scintillation Proximity Assay (SPA) (Cat.
54 #TRKQ7090, Perkin Elmer, Waltham, MA) with minor modifications. Recombinant human PDE10A
55 containing catalytic domain of human PDE10A (Swiss-Prot accession number Q9Y233) was purchased from
56
57
58
59
60

1 Enzo Life Sciences Inc., Farmingdale, NY. Recombinant human PDE3A and 3B, PDE4A and PDE4B were
2 purchased from EMD Chemicals, Inc., San Diego, CA. Optimal concentrations of enzymes were tested in the
3 linear range of the enzyme activation curves with substrate. Inhibitor compounds were tested along with
4 compound whose IC_{50} values are known (e.g.: MP-10) as an internal control for each PDE assay. All inhibitors
5 were dissolved in DMSO, and serial dilutions were performed to obtain desired concentrations. Diluted
6 compounds (10 μ L/well) were added to a 96-well plate, after addition of 50 μ L diluted PDE enzyme in buffer
7 the plate was incubated on ice for 5 min. 50 μ L of radiolabeled substrate ($[^3\text{H}]$ cAMP) at a fixed (1/3 of the K_m)
8 concentration of 1.48 kBq/mL was then added to each well and plates were incubated on ice for an additional 20
9 min to give ~30% substrate turnover before termination of the reaction with 50 μ L yttrium silicate SPA beads (8
10 mg/mL). Plates were allowed to settle for 1.5 h at rt, then counted on a Trilux Micro-Beta Counter
11 (PerkinElmer, Waltham, MA). CPM values for each well were plotted against inhibitor concentration in
12 GraphPad Prism (GraphPad Software, Inc., La Jolla, CA) and inhibitor IC_{50} values were calculated by non-
13 linear regression with Prism's one-site receptor competitive binding model. All compounds were independently
14 assayed at least twice and fitting R^2 values were $\geq 90\%$; results are reported as fitted $IC_{50} \pm \text{SD}$.

15 **Biodistribution and regional brain uptake in rats.** All animal experiments were conducted in compliance
16 with the Guidelines for the Care and Use of Research Animals under protocols approved by the Washington
17 University Animal Studies Committee. For the biodistribution studies, 1.48 – 2.22 MBq of the radiotracer was
18 injected in the tail vein of mature male Sprague-Dawley rats (250 – 400 g) under anesthesia (2.5% isoflurane in
19 oxygen). At 5, 30, and 60 min post -injection (p.i.), rats (n=4 per study group) were anesthetized and
20 euthanized. The whole brain was quickly removed and the hippocampus, striatum, cortex, thalamus, brain stem,
21 and cerebellum were separated by gross dissection. The remainder of the brain was collected to determine total
22 brain uptake. Peripheral tissues including blood, lung, heart, liver, kidney, muscle, fat, and bone were also
23 collected. Samples were weighed and counted in an automated gamma counter (Beckman Gamma 8000 well
24 counter) with a standard of diluted injectate, and the %ID/g was calculated.

25 **MicroPET brain imaging studies in male cynomolgus monkeys.** Three independent PET studies were done
26 on adult male cynomolgus macaques (~4–6 kg) for each tracer with a microPET Focus 220 scanner

1 (Concorde/CTI/Siemens Microsystems, Knoxville, TN). The animal was fasted for 12 h before PET study and
2 initially anesthetized with ketamine (10 mg/kg) and glycopyrrolate (0.13 mg/kg) intramuscularly. Upon arrival
3 at the scanner, the animal was intubated and percutaneous catheters were placed for venous tracer injection and
4 arterial blood sampling. The head was positioned supine in the adjustable head holder with the brain in the
5 center of the field of view. Anesthesia was maintained at 0.75–2.0% isoflurane in oxygen and core temperature
6 maintained at ~37 °C. A 10 min transmission scan was performed to confirm positioning; this was followed by
7 a 45 min transmission scan for attenuation correction. Subsequently, a 3 h dynamic emission scan was acquired
8 after venous injection of 185 - 259 MBq of [¹⁸F]**18d** or [¹⁸F]**20a**.

9
10 **MicroPET image processing and analysis.** Acquired list mode data were histogrammed into a 3D set of
11 sinograms and binned to the following time frames: 3 × 1 min, 4 × 2 min, 3 × 3 min, and 20 × 5 min. Sinogram
12 data were corrected for attenuation and scatter. Maximum a posteriori (MAP) reconstructions were done with
13 18 iterations and a β value of 0.004. A 1.5 mm Gaussian filter was applied to smooth each MAP reconstructed
14 image. These images were then co-registered with MRI images to accurately identify the anatomical regions of
15 interest with Amira software (Visage Imaging, Inc., Carlsbad, CA). The 3D regions of interest were manually
16 drawn through all planes of co-registered MRI images for the caudate, putamen, and cerebellum. The regions of
17 interest were then overlaid on all reconstructed PET images to obtain time-activity curves (TACs). Activity
18 measures were standardized to body weight and dose of radioactivity injected to yield standardized uptake value
19 (SUV).

20
21 **HPLC metabolite analysis of NHP plasma.** Arterial blood samples (~1.5 mL) were collected 2, 15, 30, 60 and
22 90 min p.i. from a percutaneous catheter in a heparinized syringe and 1 mL aliquots were counted in a well
23 counter then centrifuged to separate red blood cells from plasma. Plasma was deproteinated with 2 parts ice-
24 cold methanol and plasma proteins were separated by centrifugation. The solvent extract (200 μL) was injected
25 on an Agilent SB C-18 analytic HPLC column (250 mm × 4.6 mm, 5 μm), with a mobile phase of MeCN/0.1 M
26 ammonium formate buffer, pH 4.5 ([¹⁸F]**18d**, 50/50, v/v; [¹⁸F]**20a**, 52/48, v/v), flow rate 0.9 mL/min, mass
27 peaks were detected by UV at 254 nm. HPLC fractions were collected at 1 min intervals for 16 min and counted
28 on a well counter and decay-corrected. The percent parent and percent radiolabeled metabolites for [¹⁸F]**18d** and
29
30
31
32
33
34
35
36
37
38
39
40
41
42
43
44
45
46
47
48
49
50
51
52
53
54
55
56
57
58
59
60

1 [¹⁸F]**20a** was calculated by dividing the recovered activity in the respective peaks by the sum of the total
2 recovered off the column and multiplying by 100. The parent compound peaks were authenticated by co-
3 injection with the respective nonradioactive standard.
4
5
6

7 **Associated Content**

8
9 Molecular formula strings of final products and IC₅₀ values for PDEs in a csv format.
10

11 Supporting Information Table of Contents

12
13
14 General chemistry methods

15
16 Synthesis of intermediate compounds: **6a-j**, **9**, **11**, **12**, **14**, **15a-d**, and **16a-n**

17
18
19 Synthesis of radiolabeling precursors **23a-e**, **23g** and **24a** and intermediate compounds
20
21
22
23
24
25
26
27
28
29
30
31
32
33
34
35
36
37
38
39
40
41
42
43
44
45
46
47
48
49
50
51
52
53
54
55
56
57
58
59
60

Author Information

Zhude Tu, Ph.D.
Department of Radiology
Washington University School of Medicine
Campus Box 8225
510 S. Kingshighway Blvd.
St. Louis, MO 63110, USA
Tel: 1-314-362-8487
Fax: 1-314-362-8555
e-mail: tuz@mir.wustl.edu

Acknowledgement

Financial support for these studies was provided by the National Institute of Health (NIH/NINDS, NS061025, NS075527, NIH/NIMH MH092797). We would like to acknowledge the Department of Chemistry staff and the Washington University High Resolution NMR Facility for assistance with NMR spectra. Purchase of the 400 MHz NMR instrument was partially supported by S10 RR027207 from the NIH Shared Instrument Grant program. We would like to thank personnel of the Washington University Cyclotron Facility for [¹⁸F]fluoride production. We would also like to thank personnel in the East Building Imaging Research Center for technical assistance with the nonhuman primate imaging studies, and Lynne Jones, Adam Rosenberg and Xuyi Yue for assistance in editing the manuscript.

Abbreviations Used

cGMP, cyclic guanosine monophosphate; DAST, diethylaminosulfur trifluoride; DBAD, di-*tert*-butyl azodicarboxylate; DIEA, *N,N*-diisopropylethylamine; DMC, dimethyl carbonate; EOS, end of synthesis; EtOH, ethanol; EtOAc, ethyl acetate; FPEG, fluoropeGylated; MeCN, acetonitrile; MSNs, medium spiny neurons; MOM-Br, bromo(methoxy)methane; MP-10, 2-((4-(1-methyl-4-(pyridin-4-yl)-1*H*-pyrazol-3-yl)phenoxy)-methyl)quinoline; NHP, nonhuman primate; phenyl triflimide, *N*-phenyl-bis(trifluoromethane sulfonamide); PDE3A, phosphodiesterase 3A; PDE3B, phosphodiesterase 3B; PDE4A, phosphodiesterase 4A; PDE4B, phosphodiesterase 4B; PDE10A, phosphodiesterase 10A; p.i., post-injection; QC, quality control; RCY, radiochemical yield; ROI, region of interest; SA, specific activity; TBSCl, *tert*-butyldimethylsilyl chloride; TEA, triethylamine.

References

1. Soderling, S. H.; Bayuga, S. J.; Beavo, J. A. Isolation and characterization of a dual-substrate phosphodiesterase gene family: PDE10A. *Proc. Natl. Acad. Sci. USA* **1999**, *96*, 7071-7076.
2. Loughney, K.; Snyder, P. B.; Uher, L.; Rosman, G. J.; Ferguson, K.; Florio, V. A. Isolation and characterization of PDE10A, a novel human 3', 5'-cyclic nucleotide phosphodiesterase. *Gene* **1999**, *234*, 109-117.
3. Fujishige, K.; Kotera, J.; Michibata, H.; Yuasa, K.; Takebayashi, S.; Okumura, K.; Omori, K. Cloning and characterization of a novel human phosphodiesterase that hydrolyzes both cAMP and cGMP (PDE10A). *J. Biol. Chem.* **1999**, *274*, 18438-18445.
4. Fujishige, K.; Kotera, J.; Omori, K. Striatum- and testis-specific phosphodiesterase PDE10A: Isolation and characterization of a rat PDE10A. *Eur. J. Biochem.* **1999**, *266*, 1118-1127.
5. Coskran, T. M.; Morton, D.; Menniti, F. S.; Adamowicz, W. O.; Kleiman, R. J.; Ryan, A. M.; Strick, C. A.; Schmidt, C. J.; Stephenson, D. T. Immunohistochemical localization of phosphodiesterase 10A in multiple mammalian species. *J. Histochem. Cytochem.* **2006**, *54*, 1205-1213.
6. Menniti, F. S.; Faraci, W. S.; Schmidt, C. J. Phosphodiesterases in the CNS: Targets for drug development. *Nat. Rev. Drug Discovery* **2006**, *5*, 660-670.
7. Schmidt, C. J.; Chapin, D. S.; Cianfrogna, J.; Corman, M. L.; Hajos, M.; Harms, J. F.; Hoffman, W. E.; Lebel, L. A.; McCarthy, S. A.; Nelson, F. R.; Proulx-LaFrance, C.; Majchrzak, M. J.; Ramirez, A. D.; Schmidt, K.; Seymour, P. A.; Siuciak, J. A.; Tingley, F. D., 3rd; Williams, R. D.; Verhoest, P. R.; Menniti, F. S. Preclinical characterization of selective phosphodiesterase 10A inhibitors: A new therapeutic approach to the treatment of schizophrenia. *J. Pharmacol. Exp. Ther.* **2008**, *325*, 681-690.
8. Chappie, T. A.; Helal, C. J.; Hou, X. Current landscape of phosphodiesterase 10A (PDE10A) inhibition. *J. Med. Chem.* **2012**, *55*, 7299-7331.

- 1
2
3
4
5
6
7
8
9
10
11
12
13
14
15
16
17
18
19
20
21
22
23
24
25
26
27
28
29
30
31
32
33
34
35
36
37
38
39
40
41
42
43
44
45
46
47
48
49
50
51
52
53
54
55
56
57
58
59
60
9. Smith, S. M.; Uslaner, J. M.; Cox, C. D.; Huszar, S. L.; Cannon, C. E.; Vardigan, J. D.; Eddins, D.; Toolan, D. M.; Kandebo, M.; Yao, L.; Raheem, I. T.; Schreier, J. D.; Breslin, M. J.; Coleman, P. J.; Renger, J. J. The novel phosphodiesterase 10A inhibitor THPP-1 has antipsychotic-like effects in rat and improves cognition in rat and rhesus monkey. *Neuropharmacology* **2013**, *64*, 215-223.
 10. Bartolome-Nebreda, J. M.; Alonso de Diego, S. A.; Artola, M.; Delgado, F.; Delgado, O.; Martin-Martin, M. L.; Martinez-Vituro, C. M.; Pena, M. A.; Tong, H. M.; Van Gool, M.; Alonso, J. M.; Fontana, A.; Macdonald, G. J.; Megens, A.; Langlois, X.; Somers, M.; Vanhoof, G.; Conde-Ceide, S. Identification of a novel orally bioavailable phosphodiesterase 10A (PDE10A) inhibitor with efficacy in animal models of schizophrenia. *J. Med. Chem.* **2015**, *58*, 978-993.
 11. Hu, E.; Chen, N.; Bourbeau, M. P.; Harrington, P. E.; Biswas, K.; Kunz, R. K.; Andrews, K. L.; Chmait, S.; Zhao, X.; Davis, C.; Ma, J.; Shi, J.; Lester-Zeiner, D.; Danao, J.; Able, J.; Cueva, M.; Talreja, S.; Kornecook, T.; Chen, H.; Porter, A.; Hungate, R.; Treanor, J.; Allen, J. R. Discovery of clinical candidate 1-(4-(3-(4-(1*H*-benzo[*d*]imidazole-2-carbonyl)phenoxy)pyrazin-2-yl)piperidin-1-yl)ethanone (AMG 579), a potent, selective, and efficacious inhibitor of phosphodiesterase 10A (PDE10A). *J. Med. Chem.* **2014**, *57*, 6632-6641.
 12. Uthayathas, S.; Masilamoni, G. J.; Shaffer, C. L.; Schmidt, C. J.; Menniti, F. S.; Papa, S. M. Phosphodiesterase 10A inhibitor MP-10 effects in primates: Comparison with risperidone and mechanistic implications. *Neuropharmacology* **2014**, *77*, 257-267.
 13. Bartolome-Nebreda, J. M.; Delgado, F.; Martin-Martin, M. L.; Martinez-Vituro, C. M.; Pastor, J.; Tong, H. M.; Iturrino, L.; Macdonald, G. J.; Sanderson, W.; Megens, A.; Langlois, X.; Somers, M.; Vanhoof, G.; Conde-Ceide, S. Discovery of a potent, selective, and orally active phosphodiesterase 10A inhibitor for the potential treatment of schizophrenia. *J. Med. Chem.* **2014**, *57*, 4196-4212.

14. Reneerkens, O. A.; Rutten, K.; Bollen, E.; Hage, T.; Blokland, A.; Steinbusch, H. W.; Prickaerts, J. Inhibition of phosphodiesterase type 2 or type 10 reverses object memory deficits induced by scopolamine or MK-801. *Behav. Brain Res.* **2013**, *236*, 16-22.
15. Yang, S. W.; Smotryski, J.; McElroy, W. T.; Tan, Z.; Ho, G.; Tulshian, D.; Greenlee, W. J.; Guzzi, M.; Zhang, X.; Mullins, D.; Xiao, L.; Hruza, A.; Chan, T. M.; Rindgen, D.; Bleickardt, C.; Hodgson, R. Discovery of orally active pyrazoloquinolines as potent PDE10 inhibitors for the management of schizophrenia. *Bioorg. Med. Chem. Lett.* **2012**, *22*, 235-239.
16. Ho, G. D.; Yang, S. W.; Smotryski, J.; Bercovici, A.; Nechuta, T.; Smith, E. M.; McElroy, W.; Tan, Z.; Tulshian, D.; McKittrick, B.; Greenlee, W. J.; Hruza, A.; Xiao, L.; Rindgen, D.; Mullins, D.; Guzzi, M.; Zhang, X.; Bleickardt, C.; Hodgson, R. The discovery of potent, selective, and orally active pyrazoloquinolines as PDE10A inhibitors for the treatment of schizophrenia. *Bioorg. Med. Chem. Lett.* **2012**, *22*, 1019-1022.
17. Verhoest, P. R.; Chapin, D. S.; Corman, M.; Fonseca, K.; Harms, J. F.; Hou, X.; Marr, E. S.; Menniti, F. S.; Nelson, F.; O'Connor, R.; Pandit, J.; Proulx-Lafrance, C.; Schmidt, A. W.; Schmidt, C. J.; Suiciak, J. A.; Liras, S. Discovery of a novel class of phosphodiesterase 10A inhibitors and identification of clinical candidate 2-[4-(1-methyl-4-pyridin-4-yl-1H-pyrazol-3-yl)-phenoxyethyl]-quinoline (PF-2545920) for the treatment of schizophrenia. *J. Med. Chem.* **2009**, *52*, 5188-5196.
18. Schulke, J. P.; McAllister, L. A.; Geoghegan, K. F.; Parikh, V.; Chappie, T. A.; Verhoest, P. R.; Schmidt, C. J.; Johnson, D. S.; Brandon, N. J. Chemoproteomics demonstrates target engagement and exquisite selectivity of the clinical phosphodiesterase 10A inhibitor MP-10 in its native environment. *ACS Chem. Biol.* **2014**, *9*, 2823-2832.
19. Tu, Z.; Fan, J.; Li, S.; Jones, L. A.; Cui, J.; Padakanti, P. K.; Xu, J.; Zeng, D.; Shoghi, K. I.; Perlmutter, J. S.; Mach, R. H. Radiosynthesis and in vivo evaluation of [¹¹C]MP-10 as a PET probe for imaging PDE10A in rodent and non-human primate brain. *Bioorg. Med. Chem.* **2011**, *19*, 1666-1673.

- 1
2
3
4
5
6
7
8
9
10
11
12
13
14
15
16
17
18
19
20
21
22
23
24
25
26
27
28
29
30
31
32
33
34
35
36
37
38
39
40
41
42
43
44
45
46
47
48
49
50
51
52
53
54
55
56
57
58
59
60
20. Plisson, C.; Salinas, C.; Weinzimmer, D.; Labaree, D.; Lin, S. F.; Ding, Y. S.; Jakobsen, S.; Smith, P. W.; Eiji, K.; Carson, R. E.; Gunn, R. N.; Rabiner, E. A. Radiosynthesis and in vivo evaluation of [^{11}C]MP-10 as a positron emission tomography radioligand for phosphodiesterase 10A. *Nucl. Med. Biol.* **2011**, *38*, 875-884.
 21. Lin, S. F.; Labaree, D.; Chen, M. K.; Holden, D.; Gallezot, J. D.; Kapinos, M.; Teng, J. K.; Najafzadeh, S.; Plisson, C.; Rabiner, E. A.; Gunn, R. N.; Carson, R. E.; Huang, Y. Further evaluation of [^{11}C]MP-10 as a radiotracer for phosphodiesterase 10A: PET imaging study in rhesus monkeys and brain tissue metabolite analysis. *Synapse* **2015**, *69*, 86-95.
 22. Kenk, M.; Thomas, A.; Lortie, M.; Dekemp, R.; Beanlands, R. S.; Dasilva, J. N. PET measurements of cAMP-mediated phosphodiesterase-4 with (*R*)-[^{11}C]rolipram. *Curr. Radiopharm.* **2011**, *4*, 44-58.
 23. Toth, M.; Haggkvist, J.; Stepanov, V.; Takano, A.; Nakao, R.; Amini, N.; Miura, S.; Kimura, H.; Taniguchi, T.; Gulyas, B.; Halldin, C. Molecular imaging of PDE10A knockout mice with a novel PET radiotracer: [C]T-773. *Mol. Imaging Biol.* **2015**, *17*, 445-449.
 24. Hwang, D. R.; Hu, E.; Allen, J. R.; Davis, C.; Treanor, J.; Miller, S.; Chen, H.; Shi, B.; Narayanan, T. K.; Barret, O.; Alagille, D.; Yu, Z.; Slifstein, M. Radiosynthesis and initial characterization of a PDE10A specific PET tracer [^{18}F]AMG 580 in non-human primates. *Nucl. Med. Biol.* **2015**, *42*, 654-663.
 25. Chen, H.; Lester-Zeiner, D.; Shi, J.; Miller, S.; Glaus, C.; Hu, E.; Chen, N.; Able, J.; Biorn, C.; Wong, J.; Ma, J.; Michelsen, K.; Hill Della Puppa, G.; Kazules, T.; Dou, H. H.; Talreja, S.; Zhao, X.; Chen, A.; Rumfelt, S.; Kunz, R. K.; Ye, H.; Thiel, O. R.; Williamson, T.; Davis, C.; Porter, A.; Immke, D.; Allen, J. R.; Treanor, J. AMG 580: A novel small molecule phosphodiesterase 10A (PDE10A) positron emission tomography tracer. *J. Pharmacol. Exp. Ther.* **2015**, *352*, 327-37.
 26. Kehler, J.; Kilburn, J. P.; Estrada, S.; Christensen, S. R.; Wall, A.; Thibblin, A.; Lubberink, M.; Bundgaard, C.; Brennum, L. T.; Steiniger-Brach, B.; Christoffersen, C. T.; Timmermann, S.; Kreilgaard,

- 1 M.; Antoni, G.; Bang-Andersen, B.; Nielsen, J. Discovery and development of ^{11}C -Lu AE92686 as a
2 radioligand for PET imaging of phosphodiesterase 10A in the brain. *J. Nuc. Med.* **2014**, *55*, 1513-1518.
- 3
4
5
6 27. Hwang, D. R.; Hu, E.; Rumfelt, S.; Easwaramoorthy, B.; Castrillon, J.; Davis, C.; Allen, J. R.; Chen, H.;
7
8 Treanor, J.; Abi-Dargham, A.; Slifstein, M. Initial characterization of a PDE10A selective positron
9 emission tomography tracer [^{11}C]AMG 7980 in non-human primates. *Nucl. Med. Biol.* **2014**, *41*, 343-349.
- 10
11
12
13
14 28. Andres, J. I.; De Angelis, M.; Alcazar, J.; Celen, S.; Bormans, G. Recent advances in positron emission
15 tomography (PET) radiotracers for imaging phosphodiesterases. *Curr. Top. Med. Chem.* **2012**, *12*, 1224-
16
17 1236.
- 18
19
20
21
22 29. Van Laere, K.; Ahmad, R. U.; Hudyana, H.; Dubois, K.; Schmidt, M. E.; Celen, S.; Bormans, G.; Koole,
23 M. Quantification of ^{18}F -JNJ-42259152, a novel phosphodiesterase 10A PET tracer: Kinetic modeling and
24 test-retest study in human brain. *J. Nuc. Med.* **2013**, *54*, 1285-1293.
- 25
26
27
28
29
30 30. Plisson, C.; Weinzimmer, D.; Jakobsen, S.; Natesan, S.; Salinas, C.; Lin, S. F.; Labaree, D.; Zheng, M. Q.;
31 Nabulsi, N.; Marques, T. R.; Kapur, S.; Kawanishi, E.; Saijo, T.; Gunn, R. N.; Carson, R. E.; Rabiner, E.
32 A. Phosphodiesterase 10A PET radioligand development program: From pig to human. *J. Nuc. Med.*
33
34 **2014**, *55*, 595-601.
- 35
36
37
38
39
40 41. Harada, A.; Suzuki, K.; Miura, S.; Hasui, T.; Kamiguchi, N.; Ishii, T.; Taniguchi, T.; Kuroita, T.; Takano,
42 A.; Stepanov, V.; Halldin, C.; Kimura, H. Characterization of the binding properties of T-773 as a PET
43 radioligand for phosphodiesterase 10A. *Nucl. Med. Biol.* **2015**, *42*, 146-154.
- 44
45
46
47
48
49 50. Celen, S.; Koole, M.; De Angelis, M.; Sannen, I.; Chitneni, S. K.; Alcazar, J.; Dedeurwaerdere, S.;
51 Moechars, D.; Schmidt, M.; Verbruggen, A.; Langlois, X.; Van Laere, K.; Andres, J. I.; Bormans, G.
52 Preclinical evaluation of ^{18}F -JNJ41510417 as a radioligand for PET imaging of phosphodiesterase-10A in
53 the brain. *J. Nuc. Med.* **2010**, *51*, 1584-1591.
- 54
55
56
57
58
59
60

- 1
2
3
4
5
6
7
8
9
10
11
12
13
14
15
16
17
18
19
20
21
22
23
24
25
26
27
28
29
30
31
32
33
34
35
36
37
38
39
40
41
42
43
44
45
46
47
48
49
50
51
52
53
54
55
56
57
58
59
60
33. Celen, S.; Koole, M.; Ooms, M.; De Angelis, M.; Sannen, I.; Cornelis, J.; Alcazar, J.; Schmidt, M.; Verbruggen, A.; Langlois, X.; Van Laere, K.; Andres, J. I.; Bormans, G. Preclinical evaluation of [¹⁸F]JNJ42259152 as a PET tracer for PDE10A. *Neuroimage* **2013**, *82*, 13-22.
34. Fan, J.; Zhang, X.; Li, J.; Jin, H.; Padakanti, P. K.; Jones, L. A.; Flores, H. P.; Su, Y.; Perlmutter, J. S.; Tu, Z. Radiosyntheses and in vivo evaluation of carbon-11 PET tracers for PDE10A in the brain of rodent and nonhuman primate. *Bioorg. Med. Chem.* **2014**, *22*, 2648-2654.
35. Li, J.; Jin, H.; Zhou, H.; Rothfuss, J.; Tu, Z. Synthesis and *in vitro* biological evaluation of pyrazole group-containing analogues for PDE10A. *MedChemComm* **2013**, *4*, 443-449.
36. Roberts, M. J.; Bentley, M. D.; Harris, J. M. Chemistry for peptide and protein PEGylation. *Adv. Drug Delivery Rev.* **2002**, *54*, 459-476.
37. Harris, J. M.; Chess, R. B. Effect of pegylation on pharmaceuticals. *Nat. Rev. Drug Discovery* **2003**, *2*, 214-221.
38. Stephenson, K. A.; Chandra, R.; Zhuang, Z. P.; Hou, C.; Oya, S.; Kung, M. P.; Kung, H. F. Fluoro-pegylated (FPEG) imaging agents targeting A β aggregates. *Bioconjugate Chem.* **2007**, *18*, 238-246.
39. Mitsunobu, O. The use of diethyl azodicarboxylate and triphenylphosphine in synthesis and transformation of natural-products. *Synthesis* **1981**, 1-28.
40. Swain, C. G.; Rogers, R. J. Mechanism of formation of aryl fluorides from arenediazonium fluoborates. *J. Am. Chem. Soc.* **1975**, *97*, 799-800.
41. Milstein, D.; Stille, J. K. A general, selective, and facile method for ketone synthesis from acid chlorides and organotin compounds catalyzed by palladium. *J. Am. Chem. Soc.* **1978**, *100*, 3636-3638.
42. Milstein, D.; Stille, J. K. Palladium-catalyzed coupling of tetraorganotin compounds with aryl and benzyl halides - Synthetic utility and mechanism. *J. Am. Chem. Soc.* **1979**, *101*, 4992-4998.

- 1 43. Scott, W. J.; Crisp, G. T.; Stille, J. K. Palladium-catalyzed coupling of vinyl triflates with organostannanes
2 - A short synthesis of pleraplysillin-1. *J. Am. Chem. Soc.* **1984**, *106*, 4630-4632.
3
4
5
- 6 44. Kolb, H. C.; Finn, M. G.; Sharpless, K. B. Click chemistry: Diverse chemical function from a few good
7 reactions. *Angew. Chem. Int. Ed. Engl.* **2001**, *40*, 2004-2021.
8
9
10
- 11 45. Cheng, C. C.; Yan, S. J. The Friedländer synthesis of quinolines. In *Organic Reactions*, Dauben, W. G.,
12 Ed. John Wiley & Sons, Inc.: New York, New York, 1982; Vol. 28, pp 37-201.
13
14
15
16
- 17 46. Hargreaves, R. H. J.; David, C. L.; Whitesell, L. J.; Labarbera, D. V.; Jamil, A.; Chapuis, J. C.; Skibo, E.
18 B. Discovery of quinolinediones exhibiting a heat shock response and angiogenesis inhibition. *J. Med.*
19 *Chem.* **2008**, *51*, 2492-2501.
20
21
22
23
24
- 25 47. Mager, G.; Klocke, R. K.; Kux, A.; Hopp, H. W.; Hilger, H. H. Phosphodiesterase III inhibition or
26 adrenoreceptor stimulation: Milrinone as an alternative to dobutamine in the treatment of severe heart
27 failure. *Am. Heart J.* **1991**, *121*, 1974-1983.
28
29
30
31
32
33
- 34 48. Movsesian, M.; Stehlik, J.; Vandeput, F.; Bristow, M. R. Phosphodiesterase inhibition in heart failure.
35 *Heart Failure Rev.* **2009**, *14*, 255-263.
36
37
38
39
- 40 49. McPhee, I.; Cochran, S.; Houslay, M. D. The novel long PDE4A10 cyclic AMP phosphodiesterase shows
41 a pattern of expression within brain that is distinct from the long PDE4A5 and short PDE4A1 isoforms.
42 *Cell. Signalling* **2001**, *13*, 911-918.
43
44
45
46
- 47 50. Cherry, J. A.; Davis, R. L. Cyclic AMP phosphodiesterases are localized in regions of the mouse brain
48 associated with reinforcement, movement, and affect. *J. Comp. Neurol.* **1999**, *407*, 287-301.
49
50
51
52
53
54
55
56
57
58
59
60

Figure Legends

Figure 1. [^{11}C]MP-10 and previously reported ^{11}C - and ^{18}F -labeled quinoline analogs

Figure 2. Structures of new fluorine-containing quinoline analogues, [^{18}F]18a, [^{18}F]18b, [^{18}F]18c, [^{18}F]18d, [^{18}F]18e, [^{18}F]18g, and [^{18}F]20a

Figure 3. Ratios of striatum: non-target brain regions in rats. [^{18}F]18a, [^{18}F]18b, [^{18}F]18c, [^{18}F]18d, and [^{18}F]20a displayed higher target: non-target ratios than [^{18}F]18e and [^{18}F]18g at 30 min and 60 min p.i. for both striatum: cerebellum (Top panel) and striatum:cortex (Bottom panel).

Figure 4. Representative microPET studies of [^{18}F]18d and [^{18}F]20a in the brain of a male cynomolgus macaque. a) [^{18}F]18d: PET image (top left), co-registered image (top middle), MR image (top right); b) [^{18}F]20a: PET image (top left), co-registered image (top middle), MR image (top right); c) brain TACs of [^{18}F]18d; d) brain TACs of [^{18}F]20a. Both [^{18}F]18d and [^{18}F]20a gave clear visualization of the PDE10A-enriched striatum.

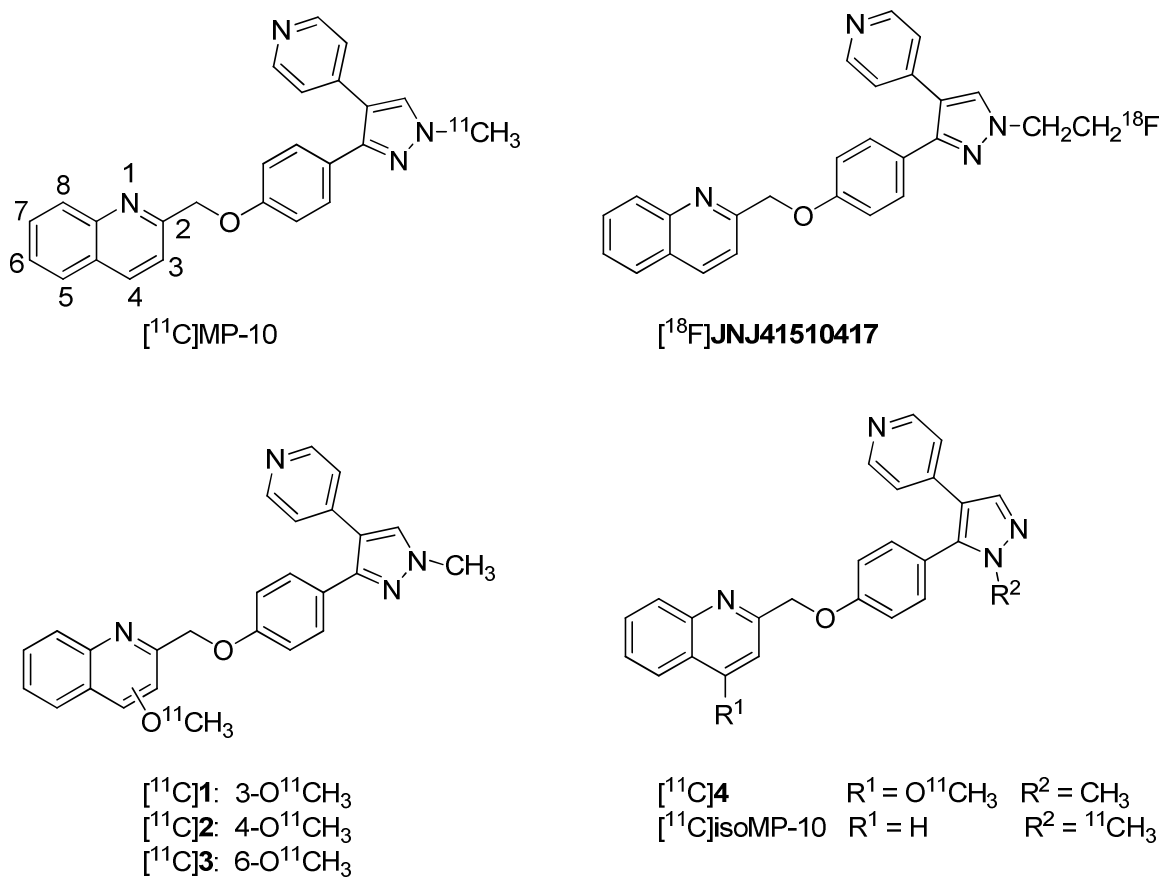


Figure 1. [¹¹C]MP-10 and previously reported ¹¹C- and ¹⁸F-labeled quinoline analogs

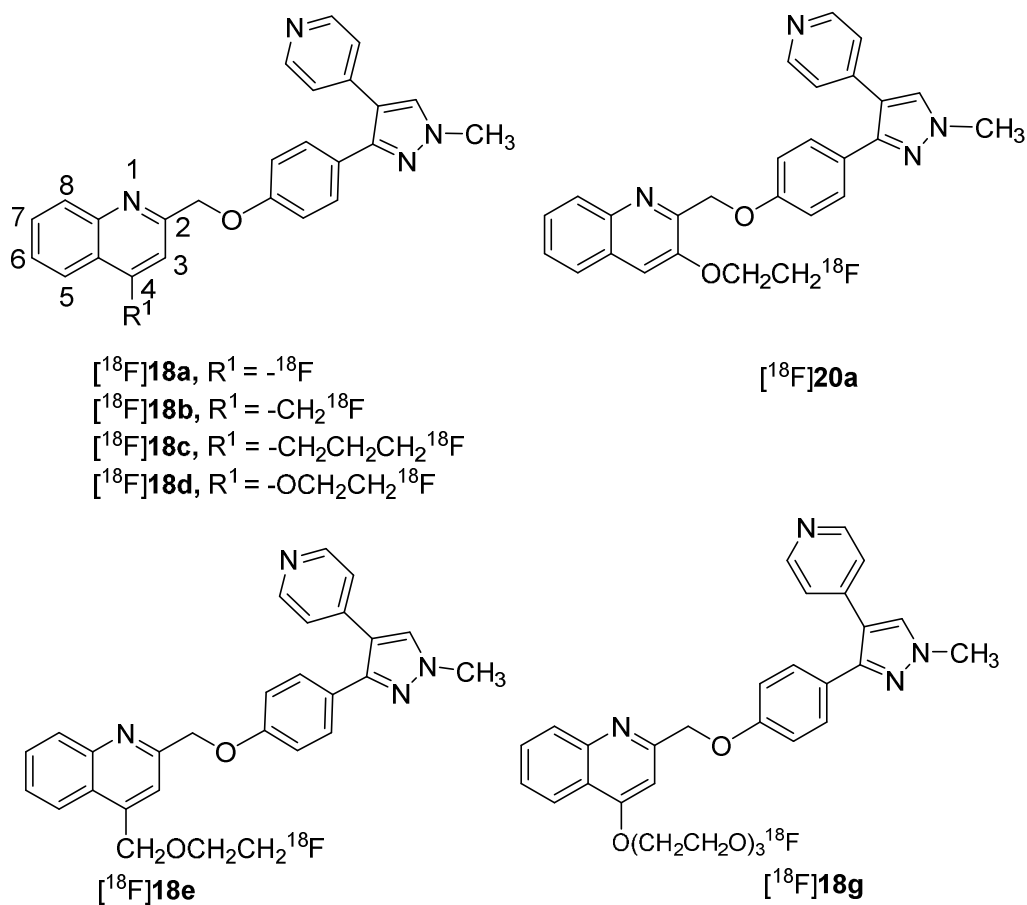


Figure 2. Structures of new fluorine-containing quinoline analogues, [¹⁸F]18a, [¹⁸F]18b, [¹⁸F]18c, [¹⁸F]18d, [¹⁸F]18e, [¹⁸F]18g, and [¹⁸F]20a.

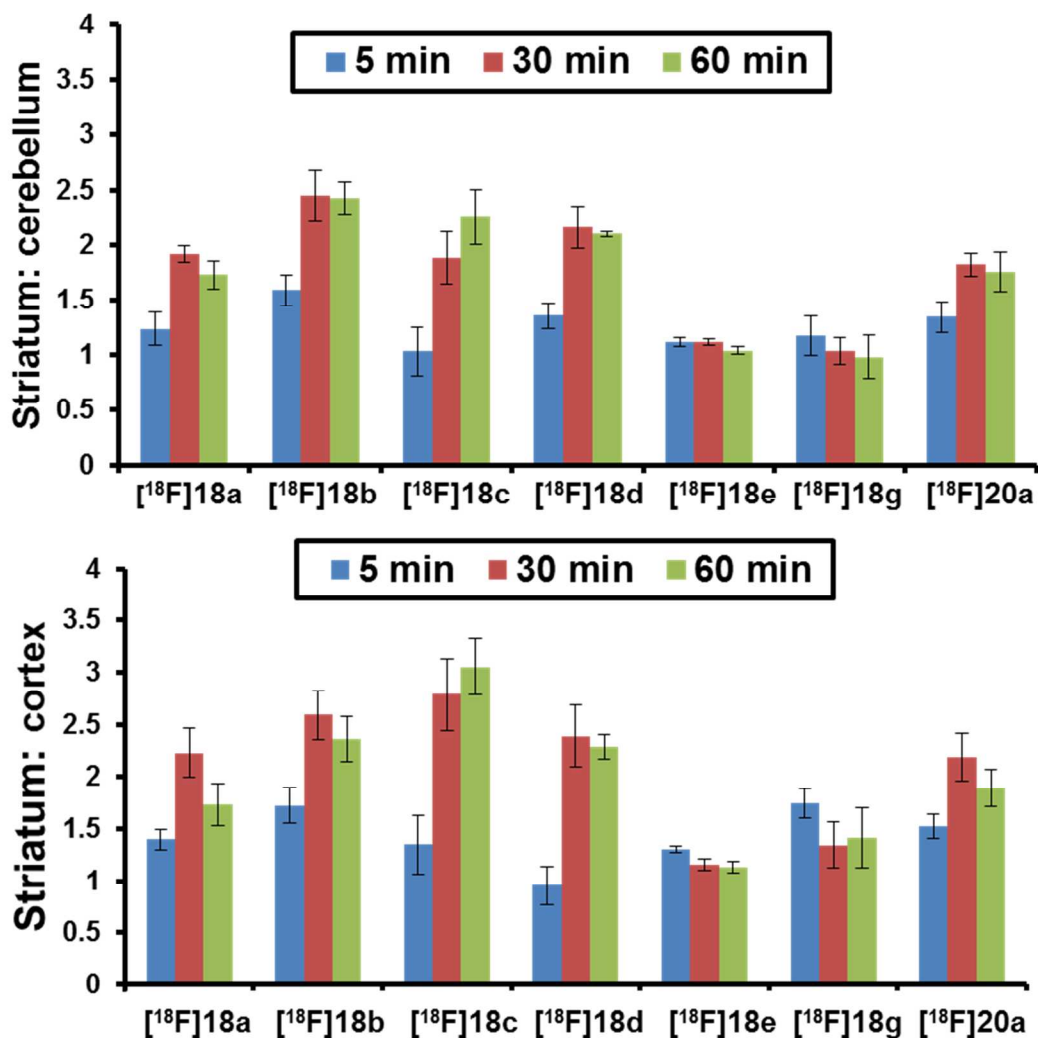


Figure 3. Ratios of striatum: non-target brain regions in rats. [¹⁸F]18a, [¹⁸F]18b, [¹⁸F]18c, [¹⁸F]18d, and [¹⁸F]20a displayed higher target: non-target ratios than [¹⁸F]18e and [¹⁸F]18g at 30 min and 60 min p.i. for both striatum: cerebellum (Top panel) and striatum:cortex (Bottom panel).

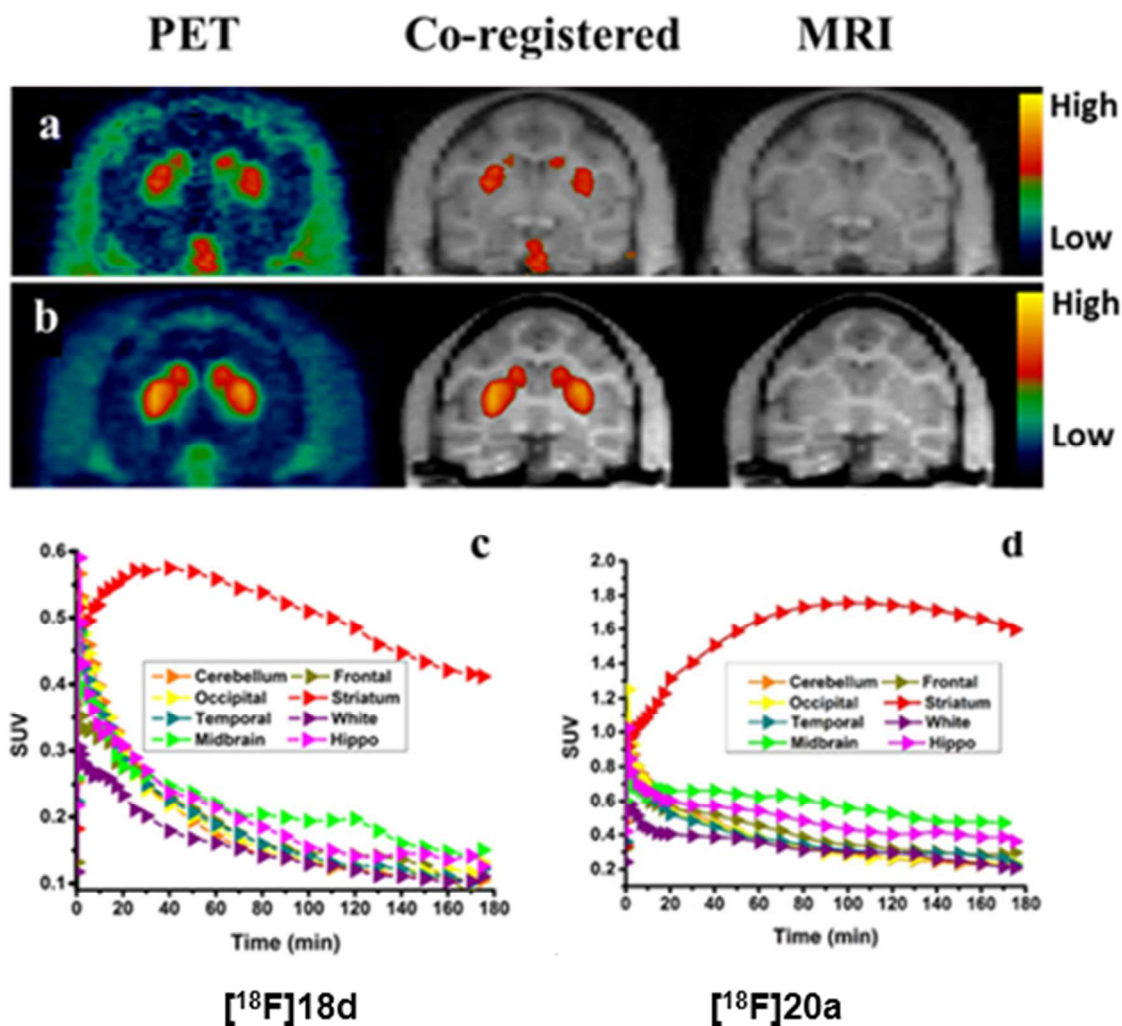
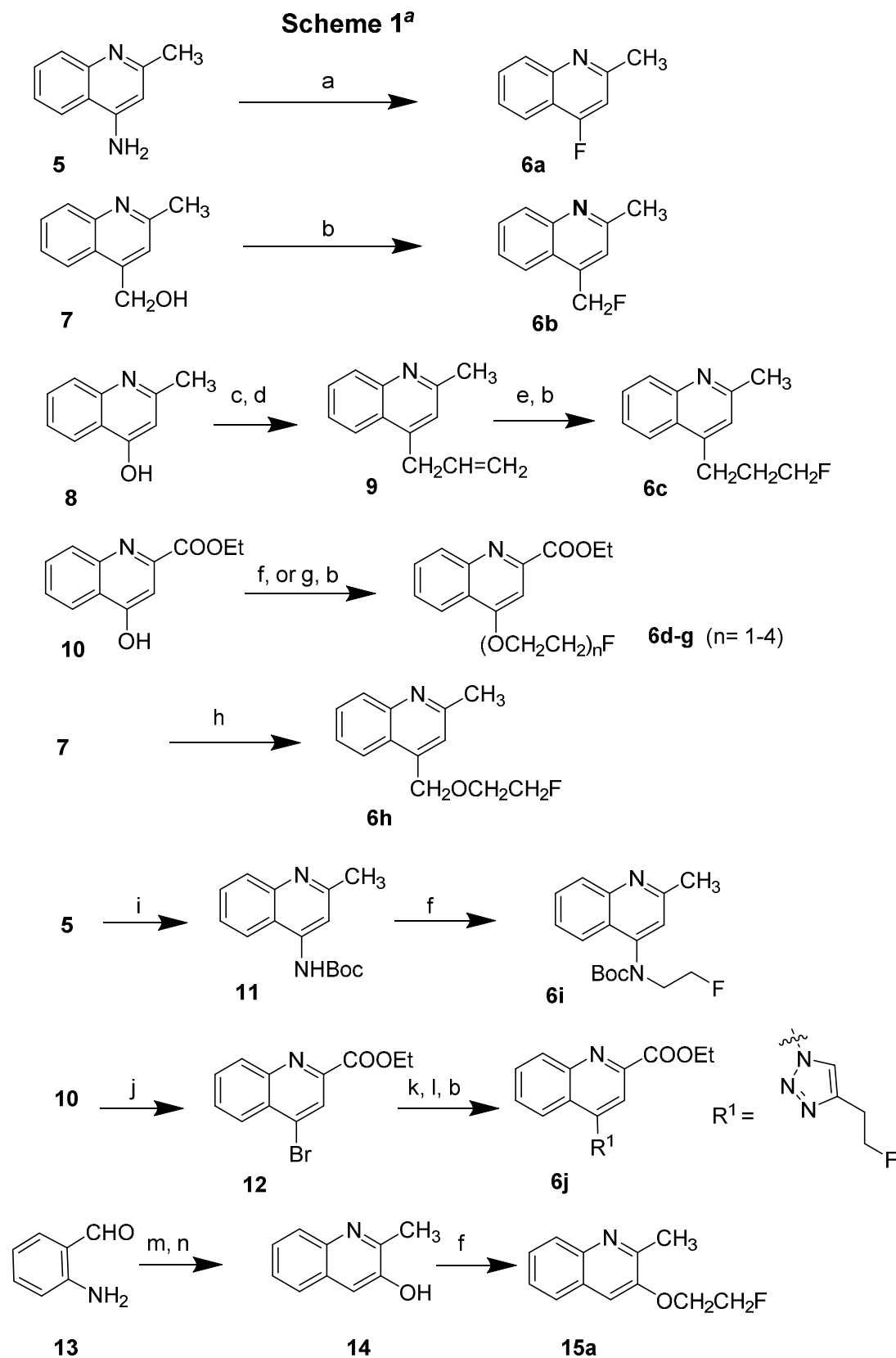


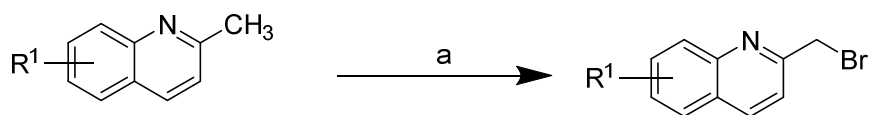
Figure 4. Representative microPET studies of $[^{18}\text{F}]\mathbf{18d}$ and $[^{18}\text{F}]\mathbf{20a}$ in the brain of a male cynomolgus macaque. a) $[^{18}\text{F}]\mathbf{18d}$: PET image (top left), co-registered image (top middle), MR image (top right); b) $[^{18}\text{F}]\mathbf{20a}$: PET image (top left), co-registered image (top middle), MR image (top right); c) brain TACs of $[^{18}\text{F}]\mathbf{18d}$; d) brain TACs of $[^{18}\text{F}]\mathbf{20a}$. Both $[^{18}\text{F}]\mathbf{18d}$ and $[^{18}\text{F}]\mathbf{20a}$ gave clear visualization of the PDE10A-enriched striatum.



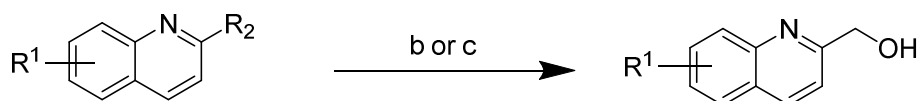
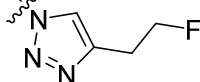
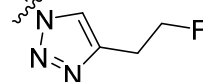
^aReagents and conditions: (a) HBF₄, NaNO₂, -10 °C to rt; (b) DAST, CH₂Cl₂, 0 °C- rt; (c) phenyl triflimide, K₂CO₃, DIPEA, MeCN, 92 °C; (d) LiBr, allyltributyltin, Pd[(C₆H₅)₃P]₄, 90 °C; (e) i) 1.0 M borane THF complex, THF, 0 °C, ii) NaOH, H₂O₂, sodium ascorbate, DMF, rt; (f) Cs₂CO₃, 1-bromo-2-fluoroethane, DMF, rt; (g) 2-(2-chloroethoxy)ethanol or 2-(2-(2-chloroethoxy)ethoxy)ethanol, K₂CO₃, DMF, 95-100 °C; or tetraethylene glycol *p*-toluenesulfonate, Cs₂CO₃, DMF, 60 °C; (h) 1-bromo-2-fluoroethane, KOH, MeCN, 80 °C; (i) (Boc)₂O, TEA, DMAP, THF, rt; (j) phosphorus(V) oxybromide, K₂CO₃, MeCN, 92 °C; (k) NaN₃, DMF, 90 °C; (l) 3-butyn-1-ol, CuSO₄·5H₂O, sodium ascorbate, DMF, rt; (m) methoxyacetone, ethanolic KOH, ethanol, reflux; (n) BBr₃, DMC, rt.

Scheme 2^a

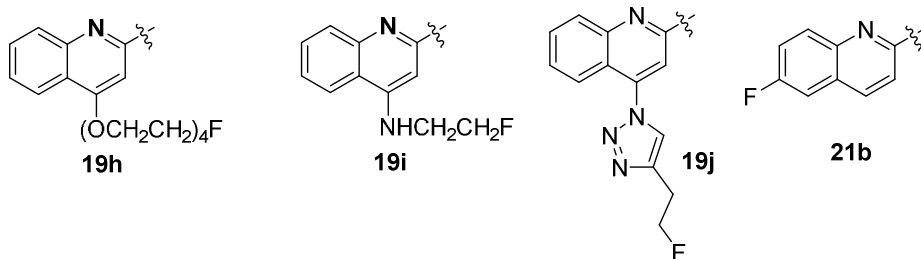
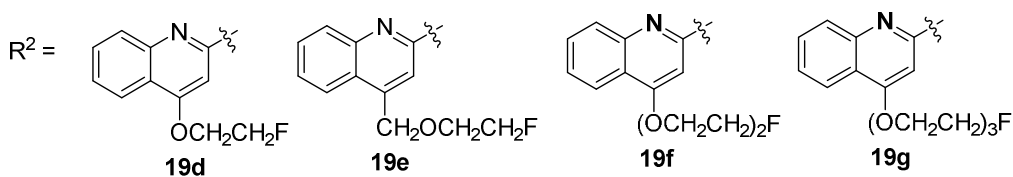
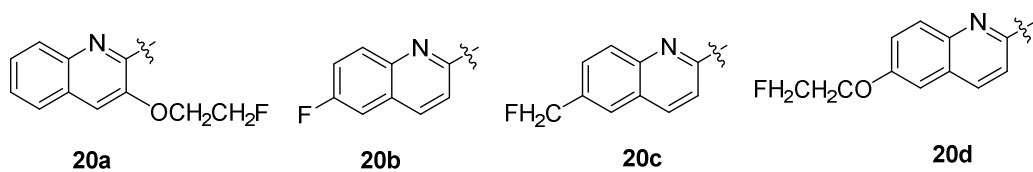
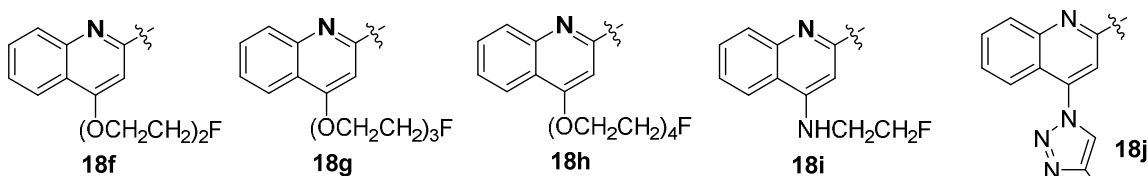
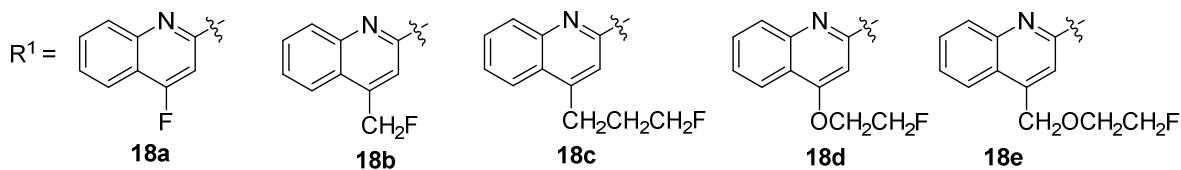
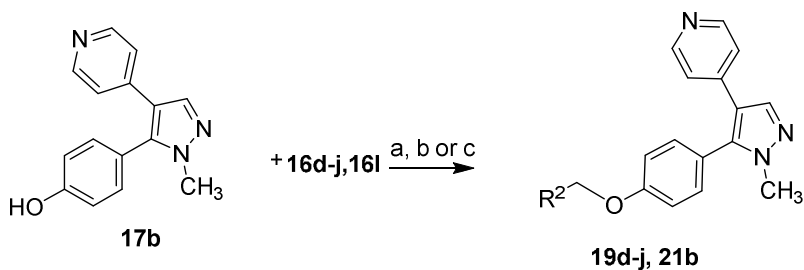
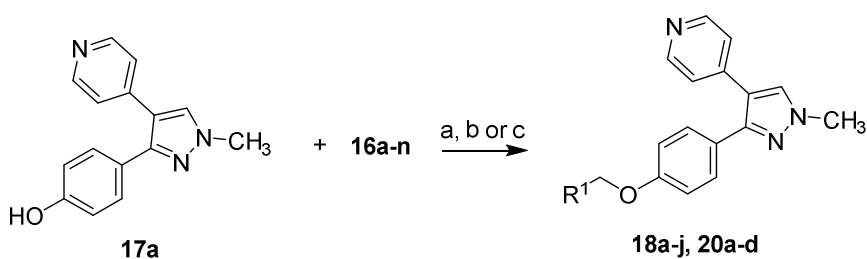
Method 1

**6a**, R¹ = 4-F**15d**, R¹ = 6-OCH₂CH₂F**16a**, R¹ = 4-F**16n**, R¹ = 6-OCH₂CH₂F

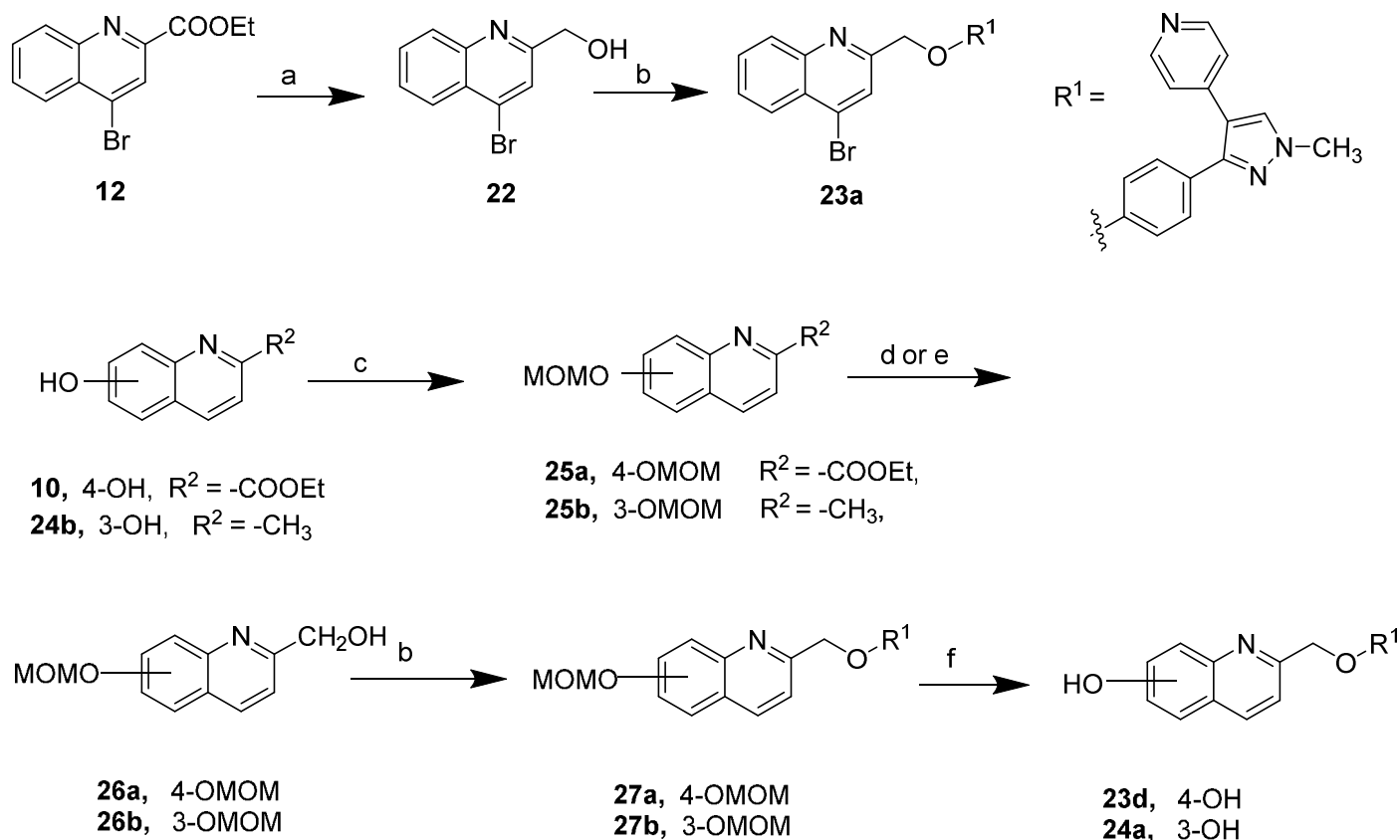
Method 2 and 3

**6b**, R² = CH₃, R¹ = 4-CH₂F**6c**, R² = CH₃, R¹ = 4-CH₂CH₂CH₂F**6d**, R² = COOEt, R¹ = 4-OCH₂CH₂F**6e**, R² = COOEt, R¹ = 4-(OCH₂CH₂)₂F**6f**, R² = COOEt, R¹ = 4-(OCH₂CH₂)₃F**6g**, R² = COOEt, R¹ = 4-(OCH₂CH₂)₄F**6h**, R² = CH₃, R¹ = 4-CH₂OCH₂CH₂F**6i**, R² = CH₃, R¹ = 4-N(Boc)CH₂CH₂F**6j**, R² = COOEt, R¹ = 4-**15a**, R² = CH₃, R¹ = 3-OCH₂CH₂F**15b**, R² = CH₃, R¹ = 6-F**15c**, R² = CH₃, R¹ = 6-CH₂F**16b**, R¹ = 4-CH₂F**16c**, R¹ = 4-CH₂CH₂CH₂F**16d**, R¹ = 4-OCH₂CH₂F**16e**, R¹ = 4-(OCH₂CH₂)₂F**16f**, R¹ = 4-(OCH₂CH₂)₃F**16g**, R¹ = 4-(OCH₂CH₂)₄F**16h**, R¹ = 4-CH₂OCH₂CH₂F**16i**, R¹ = 4-N(Boc)CH₂CH₂F**16j**, R¹ = 4-**16k**, R¹ = 3-OCH₂CH₂F**16l**, R¹ = 6-F**16m**, R¹ = 6-CH₂F

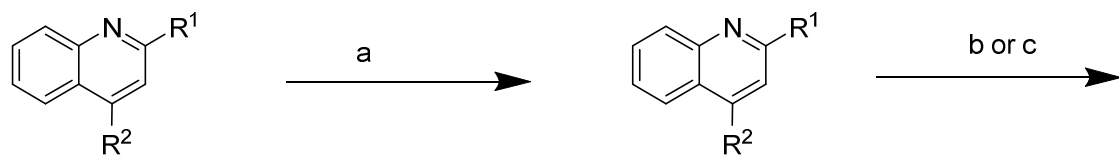
^aReagents and conditions: (a) NBS, CCl₄, reflux; (b) SeO₂, dioxane, reflux, then NaBH₄, dioxane, EtOH, rt; (c) NaBH₄, THF, MeOH, rt.

Scheme 3^a

^aReagents and conditions: (a) 17a, NaH, DMF, rt; (b) 17a or 17b, DBAD, PPh₃, dioxane, 60 °C; (c) 17a or 17b, Ph₃P, DBAD, dioxane, 60 °C; then TFA, rt.

Scheme 4^a. Synthesis of precursors (1)

^a**Reagents and conditions:** (a) $NaBH_4$, THF: MeOH (20: 1), 0 °C to r.t.; (b) **17a**, DBAD, PPh_3 , dioxane, 60 °C; (c) MOM-Br, DIPEA, CH_2Cl_2 , 0 °C; (d) SeO_2 , dioxane, reflux, then $NaBH_4$, dioxane, EtOH, rt. (e) $NaBH_4$, THF/MeOH; (f) TFA, DCM.

Scheme 5^a. Synthesis of precursors (2)

28a, R¹ = CH₃, R² = CH₂OH

28b, R¹ = CH₃, R² = (CH₂)₃OH

28c, R¹ = CH₃, R² = CH₂O(CH₂)₂OH

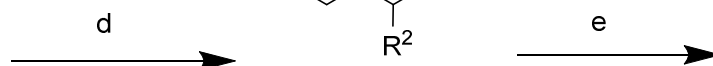
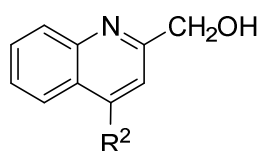
28d, R¹ = COOEt, R² = O(CH₂CH₂O)₃H

29a, R¹ = CH₃, R² = CH₂OTBS

29b, R¹ = CH₃, R² = (CH₂)₃OTBS

29c, R¹ = CH₃, R² = CH₂O(CH₂)₂OTBS

29d, R¹ = COOEt, R² = O(CH₂CH₂O)₃TBS



30a, R² = CH₂OTBS

30b, R² = (CH₂)₃OTBS

30c, R² = CH₂O(CH₂)₂OTBS

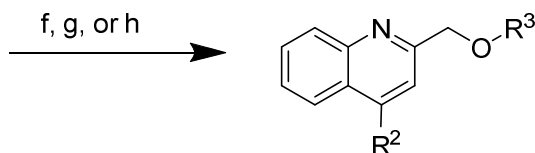
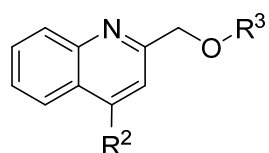
30d, R² = O(CH₂CH₂O)₃TBS

31a, R² = CH₂OTBS

31b, R² = (CH₂)₃OTBS

31c, R² = CH₂O(CH₂)₂OTBS

31d, R² = O(CH₂CH₂O)₃TBS



32a, R² = CH₂OH

32b, R² = (CH₂)₃OH

32c, R² = CH₂O(CH₂)₂OH

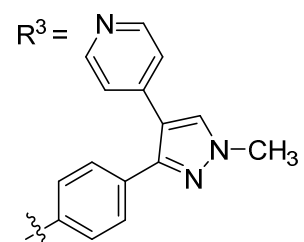
32d, R² = O(CH₂CH₂O)₃H

23b, R² = CH₂Cl

23c, R² = (CH₂)₃OMs

23e, R² = CH₂O(CH₂)₂OMs

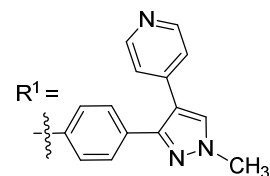
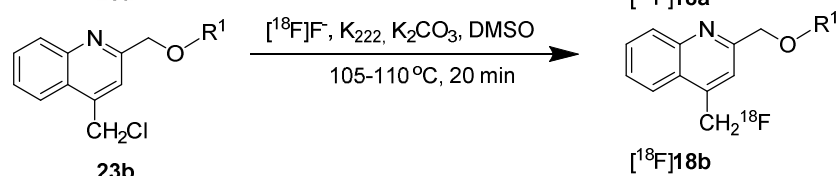
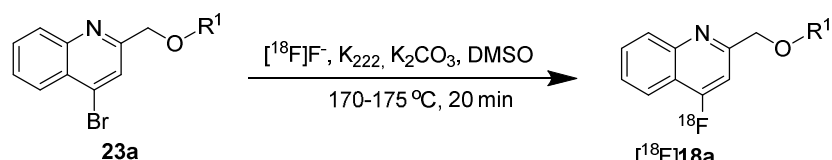
23g, R² = O(CH₂CH₂O)₃Ts



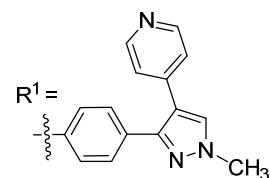
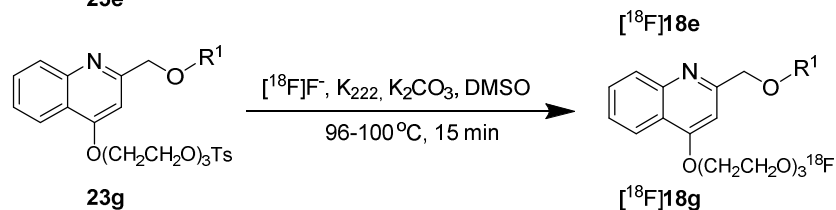
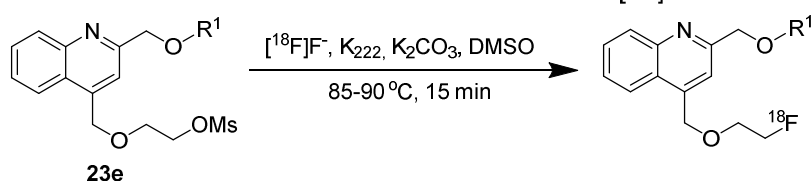
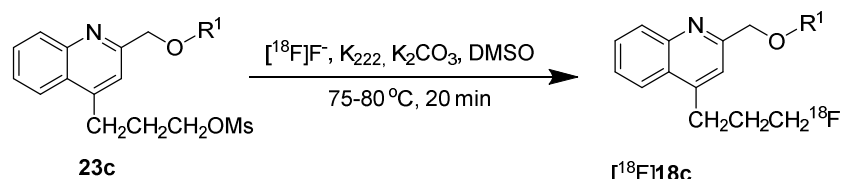
^a**Reagents and conditions:** (a) imidazole, TBSCl, DMF, 80 °C; (b) SeO₂, dioxane, reflux, then NaBH₄, dioxane, EtOH, rt.; (c) NaBH₄, THF, MeOH, rt.; (d) **17a**, Ph₃P, DBAD, dioxane, 60 °C; (e) TBAF, THF, rt; (f) SOCl₂, chloroform, 0 °C; (g) MsCl, TEA, CH₂Cl₂; (h) Ts-Cl, DMAP, DIEA, CH₂Cl₂.

Scheme 6. Radiosynthesis

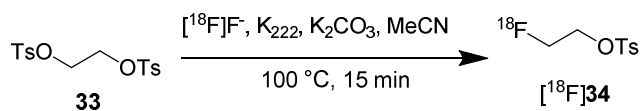
I - One-step halogen exchange



II - One-step displacement of mesylate or tosylate



III - Two-step radiosynthesis

Step 1: ¹⁸F-labeling ditosylate

Step 2: nucleophilic substitution

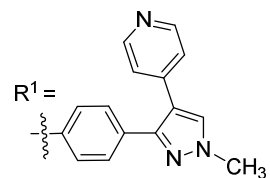
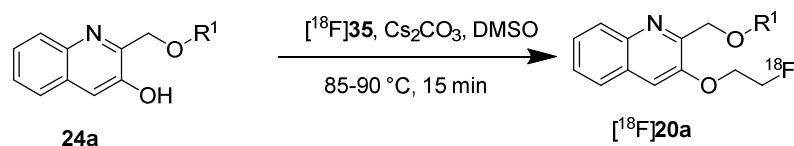
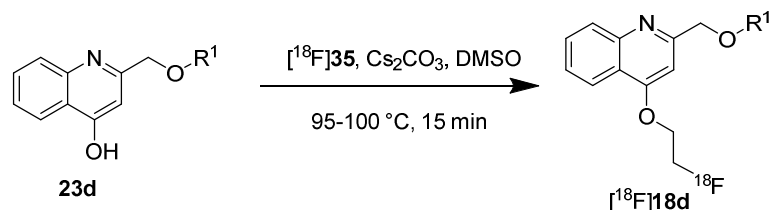
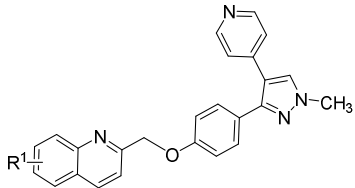
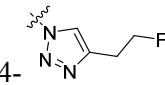
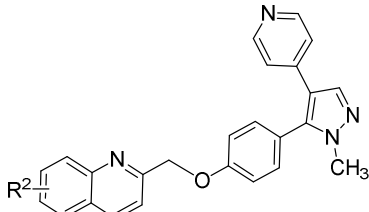
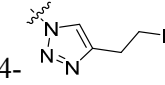


Table 1. PDE10A, PDE3A/B and PDE4A/B potency (IC_{50}) of fluorinated MP-10 analogues^a

							
Compd.	R ¹	PDE10A (nM)	PDE3A (nM × 10 ³)	PDE3B (nM × 10 ³)	PDE4A (nM × 10 ³)	PDE4B (nM × 10 ³)	LogD (7.4) ^c
18a	4-F	0.71 ± 0.12	199 ± 16.0	103 ± 10.0	8.35 ± 0.60	6.42 ± 0.27	3.47
18b	4-CH ₂ F	0.68 ± 0.02	7.71 ± 0.30	5.68 ± 0.25	4.09 ± 0.25	3.80 ± 0.15	3.75
18c	4-CH ₂ CH ₂ CH ₂ F	1.80 ± 0.09	21.9 ± 1.60	19.1 ± 3.0	0.46 ± 0.03	0.38 ± 0.03	4.43
18d	4-OCH ₂ CH ₂ F	0.32 ± 0.18	29.5 ± 0.23	7.76 ± 0.11	1.01 ± 0.14	1.77 ± 0.16	4.02
18e	4-CH ₂ OCH ₂ CH ₂ F	0.65 ± 0.02	4.07 ± 0.36	4.55 ± 0.23	2.22 ± 0.08	1.77 ± 0.13	3.49
18f	4-(OCH ₂ CH ₂) ₂ F	0.27 ± 0.10	22.9 ± 2.10	16.2 ± 0.93	1.44 ± 0.09	0.90 ± 0.05	3.62
18g	4-(OCH ₂ CH ₂) ₃ F	0.24 ± 0.04	116 ± 10.0	61.9 ± 4.60	1.57 ± 0.07	1.58 ± 0.08	3.26
18h	4-(OCH ₂ CH ₂) ₄ F	0.33 ± 0.07	144.4 ± 27	29.6 ± 0.27	9.89 ± 0.23	10.3 ± 0.47	2.90
18i	4-NHCH ₂ CH ₂ F	0.52 ± 0.24	3.74 ± 0.18	3.48 ± 0.66	5.97 ± 0.28	4.80 ± 0.34	3.98
18j		3.07 ± 0.27	4.51 ± 0.24	3.56 ± 0.86	1.57 ± 0.14	18.3 ± 1.7	3.37
20a	3-OCH ₂ CH ₂ F	0.26 ± 0.01	25.9 ± 3.20	19.9 ± 4.50	1.76 ± 0.11	1.04 ± 0.09	4.10
20b	6-F	0.29 ± 0.01	38.5 ± 12.0	23.9 ± 5.10	2.33 ± 0.39	2.55 ± 0.26	3.60
20c	6-CH ₂ F	>76	ND ^b	ND ^b	ND ^b	ND ^b	3.75
20d	6-OCH ₂ CH ₂ F	33.5 ± 0.81	ND ^b	ND ^b	ND ^b	ND ^b	3.84
							
Compd.	R ²	PDE10A (nM)	PDE3A (nM × 10 ³)	PDE3B (nM × 10 ³)	PDE4A (nM × 10 ³)	PDE4B (nM × 10 ³)	LogD (7.4) ^c
19d	4-OCH ₂ CH ₂ F	1.16 ± 0.43	3.77 ± 0.36	5.61 ± 3.10	3.72 ± 0.45	1.02 ± 0.06	4.01
19e	4-CH ₂ OCH ₂ CH ₂ F	1.12 ± 0.51	306 ± 36	>1000	4.77 ± 0.16	4.24 ± 0.20	3.49
19f	4-(OCH ₂ CH ₂) ₂ F	0.36 ± 0.15	66.4 ± 4.40	50.1 ± 3.00	12.3 ± 0.70	11.6 ± 0.67	3.62
19g	4-(OCH ₂ CH ₂) ₃ F	0.47 ± 0.09	62.2 ± 5.30	51.8 ± 4.00	8.36 ± 0.03	7.31 ± 0.32	3.26
19h	4-(OCH ₂ CH ₂) ₄ F	0.30 ± 0.03	58.71 ± 2.0	28.13 ± 1.9	15.0 ± 2.80	1.73 ± 0.18	2.90
19i	4-NHCH ₂ CH ₂ F	0.37 ± 0.09	78.8 ± 15.0	38.3 ± 6.0	12.4 ± 2.40	1.59 ± 0.19	3.98
19j		4.98 ± 0.45	0.81 ± 0.01	16.2 ± 8.00	1.86 ± 0.32	0.90 ± 0.09	3.37
21b	6-F	0.76 ± 0.12	111 ± 38.0	151 ± 37	9.73 ± 1.50	0.76 ± 0.07	3.60

^a IC_{50} is defined as the concentration of the inhibitor required to reduce the [³H]cAMP hydrolysis of recombinant human PED10A, PDE3A/3B, or PDE4A/4B by 50% in a scintillation proximity assay.

^b Not determined

^c Calculated Log D value at pH 7.4, ACD/I-Lab ver. 7.0 (Advanced Chemistry Development, Inc. Toronto, Ontario, Canada).

Table 2. Biodistribution of [¹⁸F]18a, [¹⁸F]18b, [¹⁸F]18c, [¹⁸F]18d, [¹⁸F]18e, [¹⁸F]18g and [¹⁸F]20a in male Sprague Dawley rats^a

Organ	5 min	30 min	60 min	5 min	30 min	60 min	
		[¹⁸F]18a			[¹⁸F]18b		
Blood	0.353 ± 0.063	0.376 ± 0.033	0.150 ± 0.021	0.471 ± 0.040	0.416 ± 0.062	0.201 ± 0.026	
Liver	6.87 ± 1.27	3.00 ± 0.91	1.60 ± 0.87	10.16 ± 1.86	4.01 ± 1.34	3.10 ± 0.61	
Kidney	1.887 ± 0.296	1.034 ± 0.131	0.533 ± 0.119	1.799 ± 0.207	1.351 ± 0.216	0.573 ± 0.134	
Muscle	0.339 ± 0.053	0.236 ± 0.019	0.092 ± 0.010	0.227 ± 0.042	0.174 ± 0.042	0.107 ± 0.032	
Fat	0.404 ± 0.102	0.576 ± 0.154	0.477 ± 0.099	0.343 ± 0.153	0.352 ± 0.081	0.222 ± 0.029	
Bone	0.522 ± 0.116	4.035 ± 0.153	6.300 ± 0.314	0.421 ± 0.063	4.055 ± 1.305	5.620 ± 1.132	
Brain	0.410 ± 0.063	0.191 ± 0.036	0.125 ± 0.009	0.128 ± 0.012	0.094 ± 0.023	0.069 ± 0.008	
		[¹⁸F]18c			[¹⁸F]18d		
Blood	0.459 ± 0.049	0.345 ± 0.043	0.345 ± 0.043	0.362 ± 0.048	0.226 ± 0.073	0.215 ± 0.008	
Liver	9.99 ± 1.27	5.67 ± 0.73	6.79 ± 2.49	6.88 ± 1.15	6.98 ± 0.99	3.29 ± 0.56	
Kidney	2.471 ± 0.487	1.364 ± 0.077	1.216 ± 0.180	2.200 ± 0.158	1.055 ± 0.218	0.765 ± 0.153	
Muscle	0.223 ± 0.067	0.178 ± 0.016	0.103 ± 0.030	0.247 ± 0.031	0.134 ± 0.019	0.132 ± 0.011	
Fat	0.220 ± 0.100	0.491 ± 0.035	0.368 ± 0.077	0.213 ± 0.007	0.302 ± 0.033	0.259 ± 0.025	
Bone	0.222 ± 0.014	1.418 ± 0.182	2.037 ± 0.303	0.189 ± 0.004	0.091 ± 0.012	0.142 ± 0.001	
Brain	0.114 ± 0.015	0.046 ± 0.006	0.026 ± 0.005	0.118 ± 0.012	0.078 ± 0.009	0.101 ± 0.002	
		[¹⁸F]18e			[¹⁸F]18g		
Blood	0.440 ± 0.038	0.424 ± 0.074	0.401 ± 0.029	0.699 ± 0.090	0.771 ± 0.061	0.646 ± 0.045	
Liver	3.99 ± 0.82	0.987 ± 0.038	0.554 ± 0.064	4.74 ± 1.10	1.53 ± 0.49	0.527 ± 0.068	
Kidney	0.981 ± 0.163	0.632 ± 0.123	0.485 ± 0.045	5.969 ± 0.744	1.793 ± 0.291	1.037 ± 0.170	
Muscle	0.155 ± 0.040	0.265 ± 0.117	0.228 ± 0.058	0.419 ± 0.090	0.488 ± 0.086	0.379 ± 0.027	
Fat	0.139 ± 0.031	0.139 ± 0.037	0.066 ± 0.018	0.225 ± 0.086	0.254 ± 0.051	0.123 ± 0.021	
Bone	0.133 ± 0.028	0.170 ± 0.030	0.337 ± 0.072	0.487 ± 0.044	0.441 ± 0.049	0.490 ± 0.035	
Brain	0.213 ± 0.039	0.353 ± 0.021	0.343 ± 0.033	0.353 ± 0.052	0.509 ± 0.038	0.421 ± 0.028	
		[¹⁸F]20a					
Blood	0.343 ± 0.061	0.306 ± 0.016	0.287 ± 0.010				
Liver	4.24 ± 0.74	3.17 ± 0.55	1.80 ± 0.62				
Kidney	1.789 ± 0.332	1.022 ± 0.103	0.841 ± 0.087				
Muscle	0.166 ± 0.017	0.156 ± 0.014	0.134 ± 0.009				
Fat	0.119 ± 0.021	0.202 ± 0.023	0.124 ± 0.011				
Bone	0.182 ± 0.003	0.144 ± 0.006	0.224 ± 0.015				
Brain	0.092 ± 0.011	0.129 ± 0.005	0.149 ± 0.013				

^a%ID/g values (mean ± SD) with n = 4 rats per group.

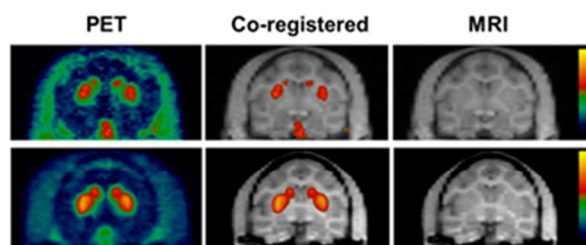
Table 3. HPLC analysis of NHP plasma for [^{18}F]18d and [^{18}F]20a

Tracer	Time p.i. (min)	% Peak 1 ^a	% Peak 2 ^b	% Parent
[^{18}F]18d	2	1	0	98
	15	4	0	93
	30	7	1	90
	60	19	5	75
	90	32	9	57
[^{18}F]20a	2	0	0	99
	15	6	2	90
	30	15	8	73
	60	29	14	55
	90	39	14	45

^a Peak 1 (radiometabolite) retention time ~3.5 min

^b Peak 2 (radiometabolite) retention time ~ 7.5 min

Table of Contents graphic



Top panel- ^{18}F 18d ($\text{IC}_{50_PDE10A} = 0.32 \pm 0.18 \text{ nM}$)
Bottom panel- ^{18}F 20a ($\text{IC}_{50_PDE10A} = 0.26 \pm 0.01 \text{ nM}$)

Table of Contents Graphic

